Charting the Normal Development of Structural Brain Connectivity in Utero using Diffusion MRI

Davood Karimi[1*], Bo Li[1*], Athena Taymourtash[2],
Camilo Jaimes[3], Ellen P. Grant[1], Simon K. Warfield[1]
[1] Department of Radiology, Harvard Medical School and Boston Children's Hospital, Boston, Massachusetts, USA
[2] Electrical Engineering and Computer Science, Massachusetts Institute of Technology, Cambridge, Massachusetts, USA
[3] Department of Radiology, Harvard Medical School and Massachusetts General Hospital, Boston, Massachusetts, USA
[*] These authors contributed equally to this work.

September 2025

Abstract

Understanding the structural connectivity of the human brain during fetal life is essential for uncovering the early foundations of neural function and vulnerability to developmental disorders. Diffusion-weighted MRI (dMRI) enables noninvasive mapping of white-matter pathways and construction of the brain's structural connectome, but its application to the fetal brain has been constrained by limited data and the technical challenges of fetal dMRI analysis. Here, we present the largest study to date of in utero brain connectivity, analyzing high-quality dMRI data from 198 fetuses between 22 and 37 gestational weeks from the Developing Human Connectome Project. We applied advanced fetal-specific tools for brain segmentation, parcellation, and tractography, and used fiber bundle capacity to weight connections. We reconstructed individual structural connectomes and characterized their developmental trajectories. Graph-theoretical analysis revealed consistent increases in both integration and segregation metrics across gestation, alongside stable small-world properties. Bootstrapping confirmed the robustness of nodal and edge-wise developmental patterns, and a sigmoid growth model identified a narrow time window (approximately 27.5–30.5 weeks) of rapid connectivity strengthening. In addition, we introduced a new method for constructing age-specific connectome templates by aggregating individual subject connectomes. Our analysis shows that this approach outperforms spatial alignment and image-space averaging, yielding templates that preserve individual topology and support accurate age prediction. Together, these findings provide a reasonable normative map of fetal brain structural connectivity and establish a foundation for future studies of atypical development and early indicators of neurological risk.

1 Introduction

Understanding the brain's structural connectivity is a central goal in neuroscience [1–4]. The structural connectome underpins and supports all brain functions, and it both influences and is shaped by the brain's responses to disease. Diffusion-weighted MRI (dMRI) provides a unique, noninvasive means of studying this connectivity [5–8]. The dMRI signal can be used to estimate the local orientation of white-matter fibers, and tractography algorithms can then trace virtual streamlines connecting predefined brain regions. These streamlines—typically weighted using measures of tissue microstructural integrity or fiber bundle capacity—define the strengths of interregional connections used to construct a structural connectome [9–11]. The connectome can be represented as a mathematical graph, in which brain regions correspond to nodes and connections correspond to edges. Graph-theoretic metrics derived from this representation enable quantitative analysis of the connectome's organization [4, 6, 12].

Although dMRI-based connectivity analysis faces several technical challenges, ongoing methodological advances have steadily improved its accuracy and reproducibility [11, 13, 14]. In addition, our understanding of the method's capabilities and limitations has matured considerably, allowing for more reliable interpretation of quantitative results [15–18]. Numerous studies have used structural connectivity to investigate brain development, aging, and degeneration [10, 19–22]. Extensive research in adults has shown that neurological conditions such as epilepsy, dementia, Alzheimer's disease, schizophrenia, ADHD, and multiple sclerosis are strongly associated with disruptions in the structural connectome [23–34]. Collectively, these findings suggest that structural connectivity plays a central role in shaping how the brain is affected by disease and how it responds to it.

However, prior work on structural connectivity has focused almost exclusively on postnatal and adult brains, while the fetal brain has received far less attention [35–42]. This gap is due in part to the limited availability of fetal dMRI data. Although large, publicly available dMRI datasets exist for pediatric and adult populations, comparable datasets for the fetal brain have been scarce until recently. Fetal dMRI also suffers from lower signal-to-noise ratio, unpredictable motion, and typically shorter scan times [7, 43, 44]. Furthermore, the fetal brain's tissue microstructure differs substantially from that of the adult brain because of incomplete myelination and higher water content [45,46]. Rapid developmental changes further complicate analysis: white-matter tracts emerge, mature, and myelinate at distinct time points and rates throughout gestation [39, 43]. Consequently, analyzing fetal dMRI requires specialized computational methods that are not widely available. As a result, relatively little is known about how the structural connectome develops during the fetal period.

This represents a significant gap in knowledge, as the fetal period is a dynamic and critical stage of brain development [3, 35, 47–50]. Neurogenesis, neuronal migration, synapse formation, and axonal growth all begin before birth, shaping the brain's microstructure and establishing the foundations of its networks [3, 36, 51–59]. It is well established that adult-like brain structures and a highly organized connectome emerge in utero [43, 55, 58, 60–63]. Moreover, growing evidence indicates that the fetal brain's structural connectivity can be disrupted by disease and environmental influences, potentially contributing to lifelong neurodevelopmental and psychiatric disorders [48, 64–66]. For example, prenatal exposure to maternal stress, congenital heart disease, and brain malformations can alter structural connectivity in utero [38, 67–75]. Therefore, quantitative assessment of the structural connectome during the fetal period is essential for deepening our understanding of how brain networks form and develop, and may support the early identification of fetuses at elevated risk [7, 37, 74, 76, 77].

Prior studies on the fetal brain are few and face several limitations [38, 56, 74]. Most have examined small cohorts and restricted gestational age ranges. In addition, many have relied on elementary or overly simplistic computational approaches. For example, they often estimated local fiber orientations using the diffusion tensor model, which cannot resolve crossing fibers. Measures of connection strength have typically been rudimentary—such as the number of streamlines—which are known to be inadequate and biased [10,11,13]. These studies have also generally lacked microstructure-informed filtering to refine tractography. Moreover, because they relied on standard computational methods originally developed for adult brains, they are prone to suboptimal or erroneous tractography results [78,79].

In this work, we aimed to chart the development of structural connectivity during the fetal period. We used the recent release of the Developing Human Connectome Project dataset, which includes dMRI scans from approximately 250 fetuses between 22 and 37 gestational weeks [80]. We employed fetal-specific methods for tissue segmentation, parcellation, and tractography, computed a structural connectome for each fetus, and examined how connectivity metrics changed with gestational age. We assessed reproducibility using bootstrapping. In addition, we developed two approaches for constructing representative connectomes for each gestational week: one based on precise spatial alignment and averaging of imaging data, and another based on aggregating individual subject connectomes. Using these approaches, we generated age-specific connectomes that captured temporal changes in structural connectivity from 22 to 37 gestational weeks. These atlases enabled us to analyze major developmental patterns in intra- and inter-lobar connectivity within and across hemispheres. Overall, this study provides new insights into the earliest stages of structural connectome development and offers benchmarks for the normative maturation of structural connectivity during the fetal period.

2 Methods

2.1 Data and Preprocessing

This study used the fetal data from the Developing Human Connectome Project. The dataset includes 279 scans from 250 fetuses. We only considered scans with both structural (T2-weighted) and dMRI images, resulting in 259 MRI scan data from 239 fetuses. The dMRI data have been processed with the SHARD pipeline [80]. We did not perform any further preprocessing on the data, except for registering the dMRI data to the T2-weighted image for each fetus and resampling both dMRI and T2-weighted images to an isotropic voxel size of 1 mm. Quality control was performed by an expert with six years of experience in fetal dMRI analysis via visualization of diffusion tensor maps, fiber orientation maps, and whole-brain tractograms in three orthogonal views. As a result, a total of 198 scans, each from a different fetus, were selected for structural connectivity analysis in this work.

2.2 Fiber Orientation Estimation and Tractography

Each dMRI scan in this dataset consists of measurements with b=0 (n=15), b=400 (n=46), and b=1000 (n=80). As also reported in prior works [45], we found that standard multi-shell multi-tissue constrained spherical deconvolution [81] was unable to correctly estimate the partial volume fractions for white matter, gray matter, and cerebrospinal fluid (CSF) in the fetal brain. Therefore, to estimate the fiber orientation density (FOD), we used the single-shell constrained spherical deconvolution (CSD) [82], applied to the b=1000 shell data. We also computed the diffusion tensor images using the b=1000 data, which consistently produced visually superior results than with the b=400 shell data.

We applied a deep learning method [83], using the diffusion tensor image as input, to compute the tissue segmentation. Segmentation labels included white matter, cortical gray matter, subcortical gray matter, and CSF. For the cortical plate, we found that the segmentation from the T2-weighted image resulted in more accurate delineation of cortical foldings. Therefore, we combined the segmentation of the cortical plate from the T2-weighted image with segmentation of the white matter, sub-cortical gray matter, and CSF from dMRI. The same deep learning method [83] was also applied to compute a parcellation of the gray matter to define the nodes for the structural connectome.

We performed anatomically constrained tractography using the iFOD2 algorithm [84] to propagate the streamlines, with a well-tested pipeline optimized for tractography of the fetal brain in the second and third trimesters [78]. Streamline seeding was performed on all white matter voxels and also on the boundary between white matter and gray matter. We noticed that some of the tracts were more fully reconstructed by using the diffusion tensor as input while others were better reconstructed using the FOD computed with CSD. Moreover, a single setting of the angle threshold and FOD cutoff threshold was not adequate for computing all tracts. Therefore, we followed an ensemble tractography approach by choosing ten different combinations of fiber orientation inputs and the angle / FOD cutoff thresholds. Specifically, we used angle thresholds in the range $[10^\circ, 35^\circ]$ and FOD cutoff thresholds in the range $[10^{-5}, 10^{-3}]$. We computed 10^5 streamlines with each setting, for a total of 10^6 streamlines for each brain. For each brain, we computed the structural connectome using the approach proposed in [9, 85]. This approach uses the SIFT2 algorithm [86] to properly weigh the contribution of the streamlines to the structural connectivity strength.

2.3 Connectivity Metrics and Statistical Analysis

From the structural connectome of each fetus, we computed standard graph-theoretic descriptors of structural connectivity including global efficiency (GE), local efficiency (LE), characteristic path length (CPL), clustering coefficient (CC), and small-world index (SWI) [12]. We computed the strength of each node as the sum of connection strengths to all its neighbors.

We performed linear regression analyses to determine whether the connectivity metrics, the connection strength of each node, and the strength of each connectome edge (i.e., connection between each node pair) changed significantly with gestational age. For nodal strength, we additionally explored a sigmoid model, as suggested in a recent study on functional connectivity of the fetal brain [87]. This model is defined as

$$f(t) = b + \frac{L}{1 + \exp\Big[-k(t - t_0)\Big]}, \tag{1}$$

where t_0 denotes the inflection point of the model, i.e., the point of fastest increase in the connectivity strength. We used the Levenberg-Marquardt method to fit this function to data. We used the adjusted R-squared to compare the sigmoid model fit with the linear fit.

We analyzed the reproducibility of the connectomics computations via random data sampling in two ways.

1. From each scan, we used two mutually exclusive subsets of the measurements, each with seven b=0 measurements, 23 b=400 measurements, and 40 b=1000 measurements. We reconstructed the connectome and computed the connectivity metrics using each subset. We assessed the reproducibility of the quantitative connectivity analysis by comparing the intra-subject and inter-subject differences and variability in the connectome and connectivity metrics.

2. We randomly selected subsets of the subjects, performed the regression analyses described above using each subset, and analyzed the reproducibility of the results.

2.4 Computation of Age-specific Connectomes

There is usually significant inter-subject variability in neuroimaging data. Atlases are used to characterize the population averages and represent typical brain development. We aimed to compute a representative structural connectome for each gestational week between 22 and 37, at one-week intervals. Specifically, we would like to leverage the data from individual fetuses around each gestational week to compute a connectome that represents the typical connectome for that gestational week. We refer to these as "age-specific connectomes". We developed two different approaches for this purpose, one approach based on aggregating the connectomes computed for each individual fetus and another approach based on data averaging in the image space. These two approaches are described in detail below.

2.4.1 Approach 1: Connectome aggregation

In this approach, we reconstructed an age-specific connectome for each gestational week between 22 and 37 based on the connectomes computed separately for individual fetuses. Each connectome (i.e., weighted adjacency matrix) is represented as a square symmetric matrix in $\mathbb{R}^{d\times d}$, where d is the number of connectome nodes. Let us denote the set of connectomes for all N individual fetuses with $\{C_s^i\}_{i=1:N}$, where C_s^i is the *subject* connectome for fetus i. Our goal is to compute a set of representative *template* connectomes $\{C_T^j\}_{j=1:M}$, one for each of M gestational weeks. We consider three desiderata for the connectome template.

Desideratum 1- Representation We would like the representative connectome for each week to closely represent the connectome for individual fetuses with a similar gestational age. To quantify the difference between the template and individual connectomes, we use the graph edit distance (GED). The GED between two graphs C^1 and C^2 is computed as the (minimum) cost of a set of edit operations to transform one graph into another [88]. These edit operations include insertion, deletion, and substitution of either a node or an edge. In general, for arbitrary graphs, computing the exact GED is NP-hard. However, in this application all connectomes have the same fixed nodes. Therefore, GED only includes the costs associated with insertion, deletion, or substitution of edges. If we quantify the cost of each edge edit operation (i.e., edge insertion, deletion, or substitution) as the difference in edge weights due to that operation, GED will be the ℓ_1 distance between the connectomes $\text{GED}(C^1, C^2) = |C^1 - C^2|$. Therefore, we define the "representation loss" as $\mathcal{L}_{repr}(C_T|C_s) = \sum_{i=1:N}\sum_{j=1:M} G(t^i, t^j)|C_s^i - C_T^j|$. In this equation, t^i is the gestational age of subject i and t^j is that of the representative connectome C_T^j. Moreover, $G(t^i, t^j) = \exp\big(-(t^i - t^j)^2/2\sigma^2\big)$ is a Gaussian kernel that encourages similarity of age-specific representative connectomes to the individual fetuses that are closest in gestational age. Similar to prior fetal imaging studies [43, 89], we set $\sigma = 1$.

Desideratum 2- Temporal consistency. We would also like to encourage temporal consistency in the computed age-specific connectomes. To this end, we penalize the GED between the templates with close gestational weeks. Similar to the representation loss above, we use a Gaussian kernel. Hence, our proposed loss term to encourage temporal consistency of the age-specific connectomes is $\mathcal{L}_{cons}(C_T) = \sum_{j_1=1:M} \sum_{j_2=1:M} G(t^{j_1}, t^{j_2}) |C_T^{j_1} - C_T^{j_2}|$.

Desideratum 3- Preservation of long connections. Another consideration is proportional representation/preservation of long-range connections. It is known that short-range connections are more likely to be shared across different structural connectomes [90, 91]. As a result, standard methods for combining connectomes based on connection consensus are biased towards preserving more of the short-range connections and discarding the long-range connections [90]. To compensate for this inherent bias, longer connections should be preferentially preserved in order to ensure that the template/average connectome is similar to the individual subject connectomes in terms of the distribution of connection lengths. One possible approach is to use a variable consensus threshold to preferentially preserve longer connections [90]. In this work, we use the Jensen-Shannon (JS) Divergence to penalize the difference between distance-wise distribution of the connectome weights. Specifically, for an arbitrary pair of connectomes C^1 and C^2, we compute the loss function $\mathcal{L}_{JS}(C^1, C^2) = D_{JS}\big(p(C^1), p(C^2)\big)$. Here, $p(C^i)$ denotes the distance-wise distribution of the connection weights for connectome C^i, and D_{JS} is computed based on the Kullback Leibler Divergence as $D_{JS}(p, q) = D_{KL}\big(p \| (p+q)/2\big) + D_{KL}\big(q \| (p+q)/2\big)$. We approximate $p(.)$ using histograms with 20 bins. Moreover, we include a Gaussian weighting based on a similar logic as presented above for the other two loss terms. Hence, our proposed loss term is $\mathcal{L}_{dist}(C_T|C_s) = \sum_{i=1:N} \sum_{j=1:M} G(t^i, t^j) \mathcal{L}_{JS}(C_s^i, C_T^j)$.

Based on these three desiderata, we propose to compute the connectome templates by solving the following optimization problem.

$$\underset{C_T}{\text{minimize}} \quad \mathcal{L}_{repr}(C_T|C_s) + \lambda_{cons}\mathcal{L}_{cons}(C_T) + \lambda_{dist}\mathcal{L}_{dist}(C_T|C_s) \tag{2}$$

Note that in order to simplify the presentation, as in our descriptions above, in Equation (2) we have not shown the indices. To be clear, in Equation (2), $C_T \equiv \{C_T^j\}_{j=1:M}$ and $C_s \equiv \{C_s^i\}_{i=1:N}$. We solve a single optimization problem summarized in Equation (2) to recover age-specific connectomes for all M gestational weeks.

As the initial estimate to start the optimization in Equation (2), we computed C_T via simple averaging of the connectomes in each gestational week. For example, for gestational age of 30 weeks we averaged the connectomes for fetuses between 29.5 and 30.5 weeks. We then iteratively optimized C_T using stochastic gradient descent (SGD). In each optimization iteration we chose one of the subject connectomes $\{C_s^i\}_{i=1:N}$ at random and optimized C_T using SGD. We found that a small learning rate of 10^{-5} was necessary to ensure stable convergence of the optimization. Nonetheless, given the small size of the problem, the optimization was completed within a few seconds.

2.4.2 Approach 2: Data averaging in the image space

This approach is based on the precise alignment and "averaging" of the imaging data from subjects with a similar gestational age. Different steps of this approach are summarized in Figure 1. The main steps in this approach are summarized below.

1. Preprocess the structural MRI and dMRI data for each subject separately and register the dMRI to the structural MRI.

2. Divide all subjects into gestational age groups. In this work, we assigned each subject only to its closest gestational week. Specifically, all fetuses with a gestational age in the range $[t - 0.5, t + 0.5)$ were assigned to the gestational week of t. For each gestational age group:

   (a) Compute the tissue response function for each subject [96] and average them to obtain a mean response function for the age group. Use this average response function to compute the FOD

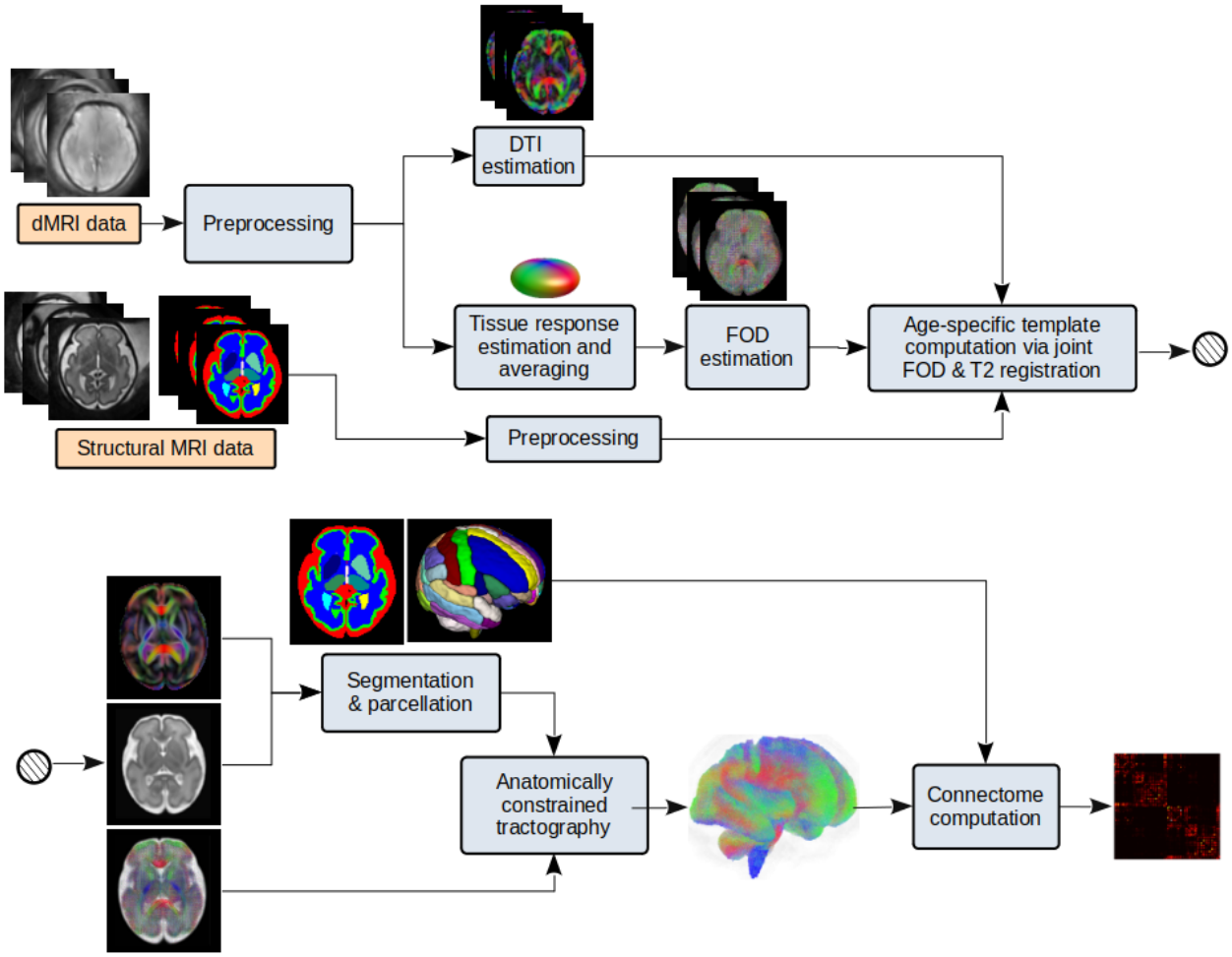

Figure 1: Image-space data averaging for computing a gestational age-specific connectome for each gestational week. Structural MRI and dMRI data from fetuses within a narrow window around the target gestational age are used as input to the pipeline. DTI and FOD maps are computed and precisely aligned using registration methods [92–94]. Segmentation/parcellation maps are computed either by fusion of subject-level data [95] or with deep learning methods [83].

map for each subject using spherical deconvolution [82]. Compute a joint structural MRI and dMRI atlas for the age group via registration of data from all subjects within the age group. This is performed using both T2-weighted images and FOD maps to align the subject imaging data [93,97]. The output of this step includes T2-weighted MRI, diffusion tensor, and FOD atlases for the gestational age group.

(b) Compute the tissue segmentation and cortex parcellation with a deep learning method [83] using the diffusion tensor atlas as input. Use the cortical plate segmentation obtained from the T2-weighted atlas to refine the tissue segmentation and parcellation maps.

(c) Compute the whole-brain tractogram based on the FOD and diffusion tensor atlases and tissue segmentation using our method described in [78]. We used an ensemble tractography approach similar to that described for individual fetuses in Section 2.2. Finally, compute the connectome.

We compared the above approaches with two existing techniques that are based on connectome aggregation [90, 91]: (1) Consensus-based thresholding, where the threshold is set such that the binary density of the connectome template is equal to the average binary density of the subject connectomes within the gestational age group. (2) Distance-preserved averaging, where different thresholds are used for different

connection lengths such that the distribution of the connection lengths in the connectome template is close to that of the subjects. Detailed descriptions of these methods are presented in [90].

We assessed the different methods by comparing the age-specific representative connectomes to the connectomes of individual subjects in two ways.

1. First, we compared scalar connectivity metrics between the representative connectomes and individual subject connectomes of the same age group.

2. Secondly, we evaluated the similarity of each individual fetal subject connectome to the connectome template of the corresponding age using a more sophisticated classification method similar to that proposed in [98]. In this approach each connectome was represented as a feature vector comprising all edge weights and eight topological descriptors. Pairwise differences between individual subject connectomes and template connectomes were summarized as the ℓ_1, ℓ_2, and ℓ_∞ norms of the differences in their feature vectors. The resulting vector of size three is regarded as the feature vector that is used by a binary support vector machine classifier. The classifier is trained to predict whether a fetus and a template belonged to the same gestational age.

3 Results and Discussion

3.1 Development of the Structural Connectivity with Gestational Age

Figure 2 illustrates whole-brain tractograms and structural connectome matrices for four fetuses at 22, 27, 32, and 37 gestational weeks. All computational steps were visually inspected by an expert with six years of experience in fetal dMRI analysis. This quality control included evaluation of color-coded fractional anisotropy maps derived from diffusion tensor imaging, fiber orientation distribution (FOD) maps computed using constrained spherical deconvolution (CSD), as well as tissue segmentation, parcellation maps, and final whole-brain tractograms. Data samples exhibiting lower image quality or clear computational errors were excluded, with the most frequent reasons being suboptimal FOD estimation or segmentation artifacts leading to implausible tractography. For comparison, Figure 3 presents age-specific average tractograms and connectomes, generated via data averaging in the image space as described in Section 2.4.2 and Figure 1.

3.1.1 Changes in the global network metrics

Figure 4 shows the developmental trajectories of several key graph-theoretical metrics – global efficiency (GE), local efficiency (LE), characteristic path length (CPL), clustering coefficient (CC), small-world index (SWI), and total network strength (defined as the sum of nodal strengths across all regions) – for individual fetuses between 22 and 37 gestational weeks. In addition to individual trajectories, the figure includes these metrics computed from two connectome templates, constructed using the methods described in Section 2.4.

Overall, the plots reveal consistent and developmentally meaningful trends. Global efficiency steadily increases while characteristic path length decreases, indicating a progressive enhancement in network integration as gestation advances. These changes suggest that the fetal brain becomes increasingly optimized for long-range communication, enabling more efficient transfer of information between anatomically distant regions. Simultaneously, both local efficiency and the clustering coefficient increase, reflecting the gradual reinforcement of short-range, locally interconnected sub-networks that support specialized functional processing. The concurrent rise in integration (GE↑, CPL↓) and segregation (LE↑, CC↑) underscores the emergence of a small–world topology, an architectural hallmark of mature and efficient neural systems that balance local specialization with global integration.

A small-world configuration refers to a network architecture that supports both local specialization and global integration with high efficiency. It is defined by (1) a high clustering coefficient, reflecting densely interconnected neighboring brain regions that support local processing, and (2) a short characteristic path length, enabling rapid communication across distant brain areas [99]. In our analysis, the small-world index (SWI) remains relatively stable across gestational ages, maintaining values in the range of 1.05–1.10. This

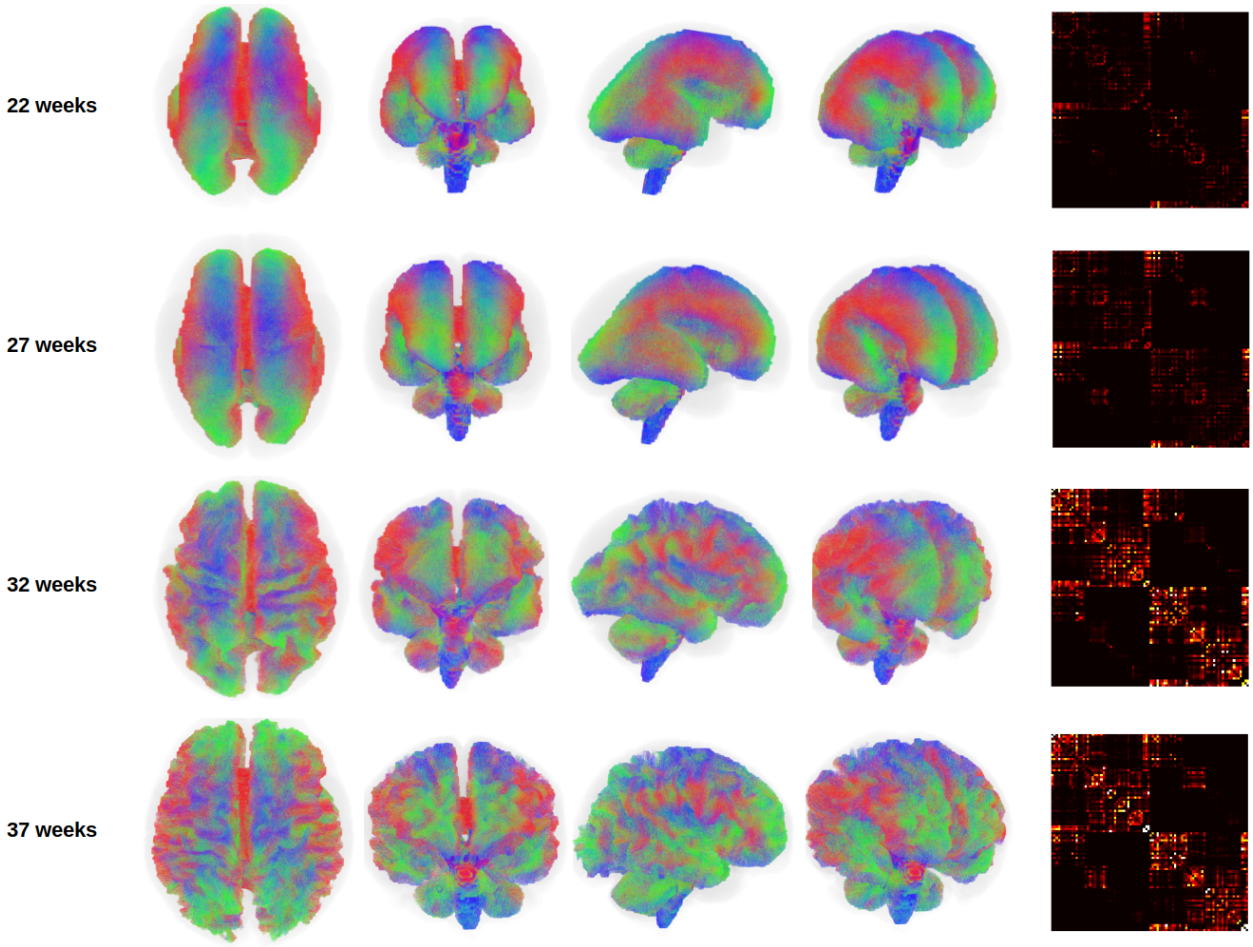

Figure 2: Different views of the whole brain tractograms, and the connectome matrices for four fetuses at different gestational ages. The tractograms for the lower gestational ages have been enlarged to the size of the higher gestational ages for better visualization. The connectomes for all gestational weeks have been shown with the same display intensity window of [0,5].

stability occurs despite simultaneous increases in both global efficiency and clustering coefficient, suggesting that the relative balance between integration and segregation is preserved during late gestation. This observation implies that the fetal brain sustains a small–world topology throughout this period, supporting the hypothesis that small–world properties are intrinsic and robust features of neural systems emerging early in development and maintained as the brain undergoes structural maturation. The preserved SWI may also indicate that the underlying developmental mechanisms scale proportionally, affecting both local and global organization in a coordinated manner.

Total network strength also shows a robust and monotonic increase with gestational age, reflecting a continuous rise in the overall connectivity of the brain. In this study, connection strength was quantified using the concept of fiber bundle capacity [9], a biologically informed metric that provides a more accurate estimate of white matter integrity and connection density than traditional measures such as streamline count. The steady increase in total strength likely mirrors the progressive development of white matter tracts, as axonal growth, myelination, and axon packing density all intensify throughout late gestation. Collectively, these findings highlight a phase of rapid and coordinated reorganization of the fetal brain's structural network, marked by increasing complexity, stronger integration, and the gradual emergence of modular substructures. This evolving architecture is well aligned with the brain's preparation for functional specialization and the demands of extra-uterine life.

Interestingly, the developmental curves computed from the connectome aggregation-based atlas closely

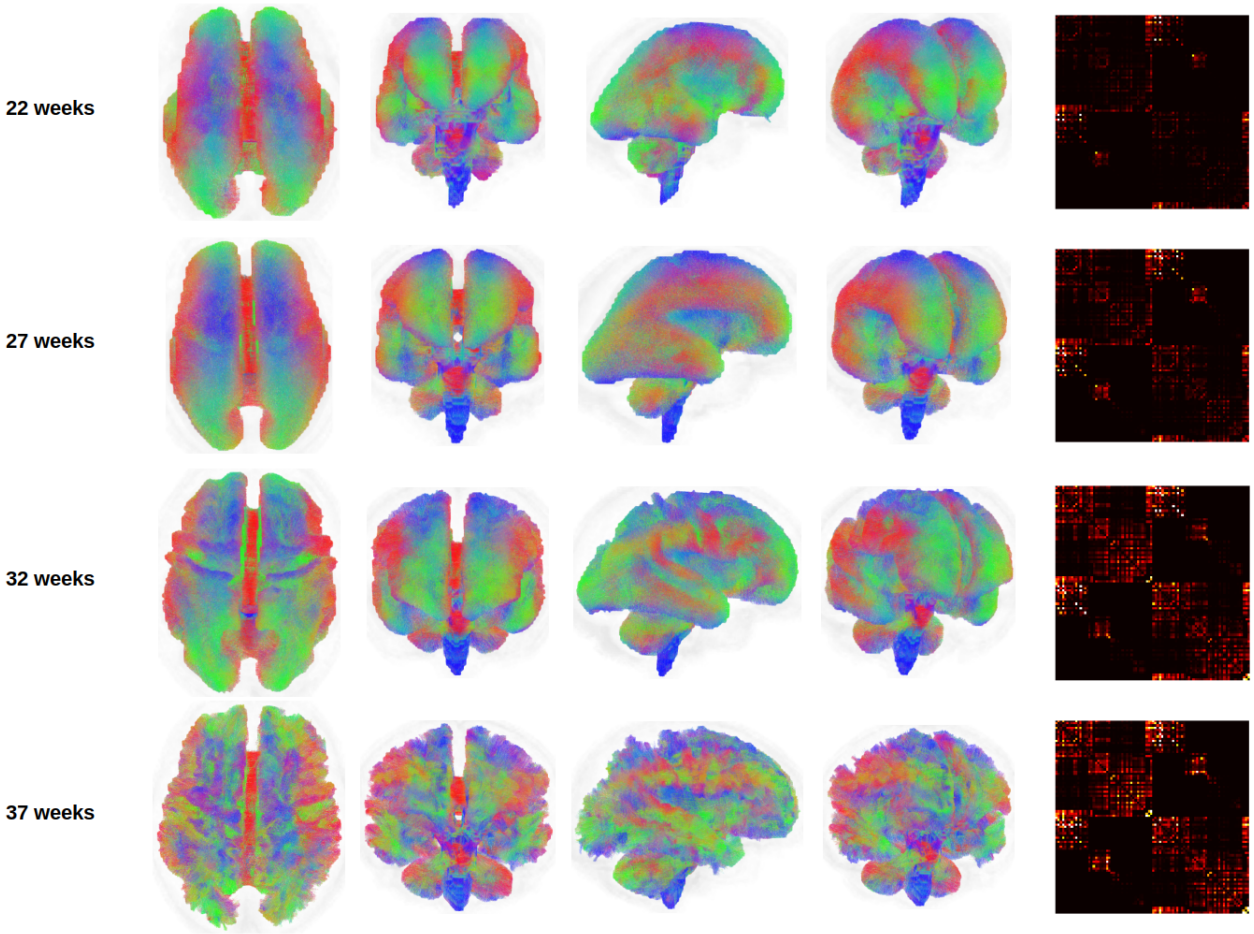

Figure 3: Tractograms and connectomes computed via data averaging in the image space, as described in Section 2.4.2, for four different gestational ages. The tractograms for the lower gestational ages have been enlarged to the size of the higher gestational ages for better visualization. The connectomes have been shown with the same display intensity window of [0,5].

mirror the average trends observed in the individual fetuses. This suggests that this method preserves the statistical and topological features of the underlying population well. In contrast, the connectome metrics computed from the template constructed via image-space averaging show notable deviations in the absolute values compared to those of individual subjects. Although the general trends with gestational age remain qualitatively consistent, the level shifts suggest that the averaging process in the image space introduces systematic alterations in the underlying connectivity patterns. This likely reflects the fact that when diffusion data from multiple fetuses (of similar gestational age) are aligned and averaged in the image space, the resulting atlas represents a spatial and microstructural average that smooths out some of the individual variability in structural connectivity. While such an atlas may offer a robust and anatomically coherent reference for the average brain at a given developmental stage, capturing shared morphological and diffusion features, it inevitably alters subject–specific details that contribute to individual connectome topology. Hence, the connectome templates obtained with this method may underrepresent inter–individual variability and distort the strength and specificity of white matter pathways. In particular, directional coherence, peak fiber density, or sharp anisotropic features that impact quantitative connectivity results may be blunted. These changes can systematically influence network topology, leading to systematic biases in graph–theoretical metric values that diverge from those observed in individual data.

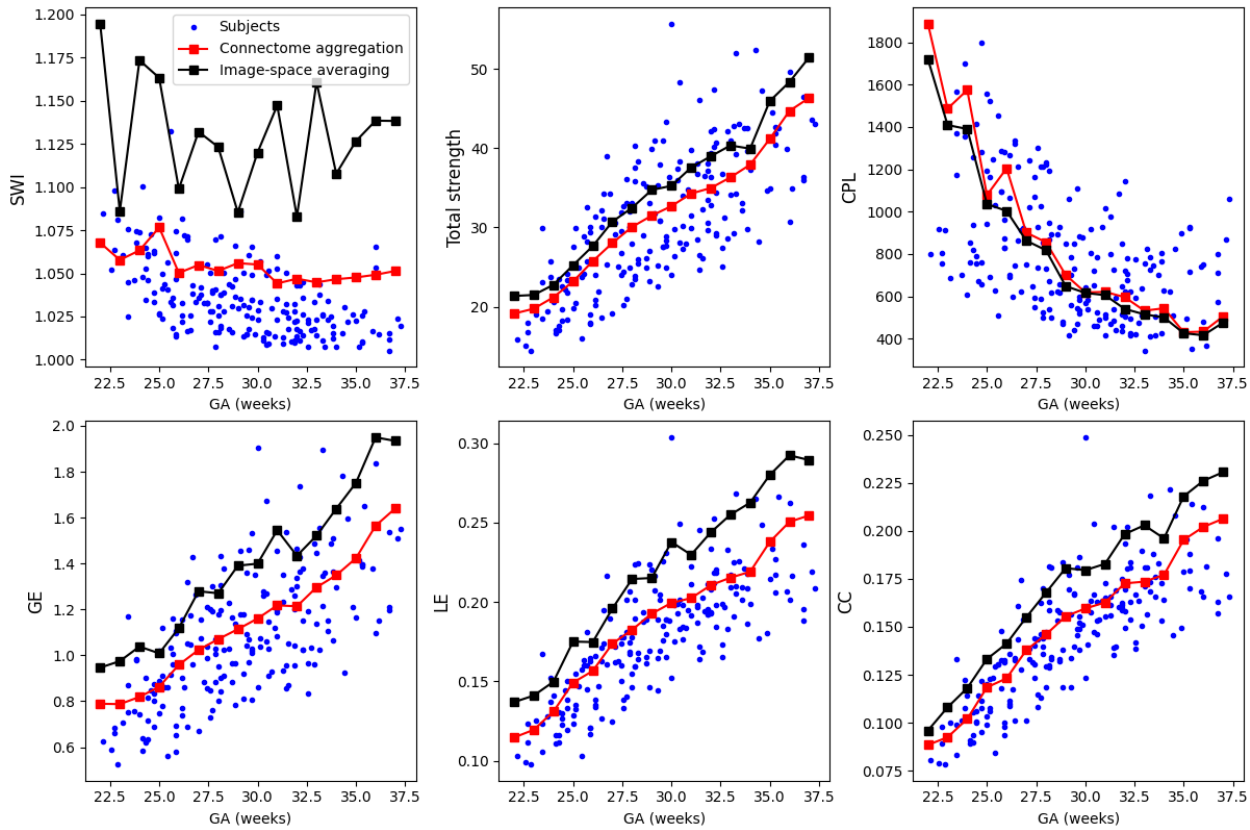

Figure 4: Plots of summary network metrics as a function of gestational age. Each plot shows the values for the subjects as blue dots and the connectome templates as red or black squares connected with line segments.

3.1.2 Changes in the nodal and edge strength with gestational age

Figure 5 displays scatter plots of nodal strength versus gestational age for each of the 88 brain regions included in the connectome. These plots illustrate a consistent developmental pattern across all nodes: nodal strength increases significantly as a function of gestational age. Linear regression analysis confirmed a statistically significant positive slope for all nodes, even under stringent control for multiple comparisons. Specifically, we used a significance threshold of $\alpha = 0.01$ and applied Bonferroni correction to account for testing across 88 regions.

To capture potential nonlinear patterns in the development of nodal strength, we fit a sigmoid growth model to the data for each brain region. Given the non-convex nature of sigmoid fitting, we employed a bootstrapped approach: the model was fit 1,000 times for each node, each iteration using a randomly selected 75% subset of the fetal subjects (without replacement). Figure 5 displays the mean of these fitted curves along with the ± 2 standard deviation confidence bounds derived across iterations. Model comparison revealed that, for most nodes, the sigmoid model outperformed a linear model in terms of adjusted R-squared, indicating a better fit to the observed data. These findings suggest that nodal strength increases in a nonlinear fashion over gestation, characterized by a period of rapid acceleration during a specific developmental window, rather than progressing uniformly across time.

We extracted the inflection point of the fitted sigmoid curve for each node, representing the gestational age at which the rate of increase in nodal strength is maximal. Across all 88 regions, inflection points ranged from 27.7 to 30.5 weeks, with a mean of 28.6 ± 0.44 weeks. When analyzed by hemisphere, both the left and right hemispheres exhibited similar but statistically distinct distributions of inflection points (28.5 ± 0.35 vs. 28.7 ± 0.50 weeks, respectively), with a paired t-test revealing a significant difference ($p = 0.00012$). We also compared the slope of the sigmoid curve at the inflection point, quantified by the inverse of the

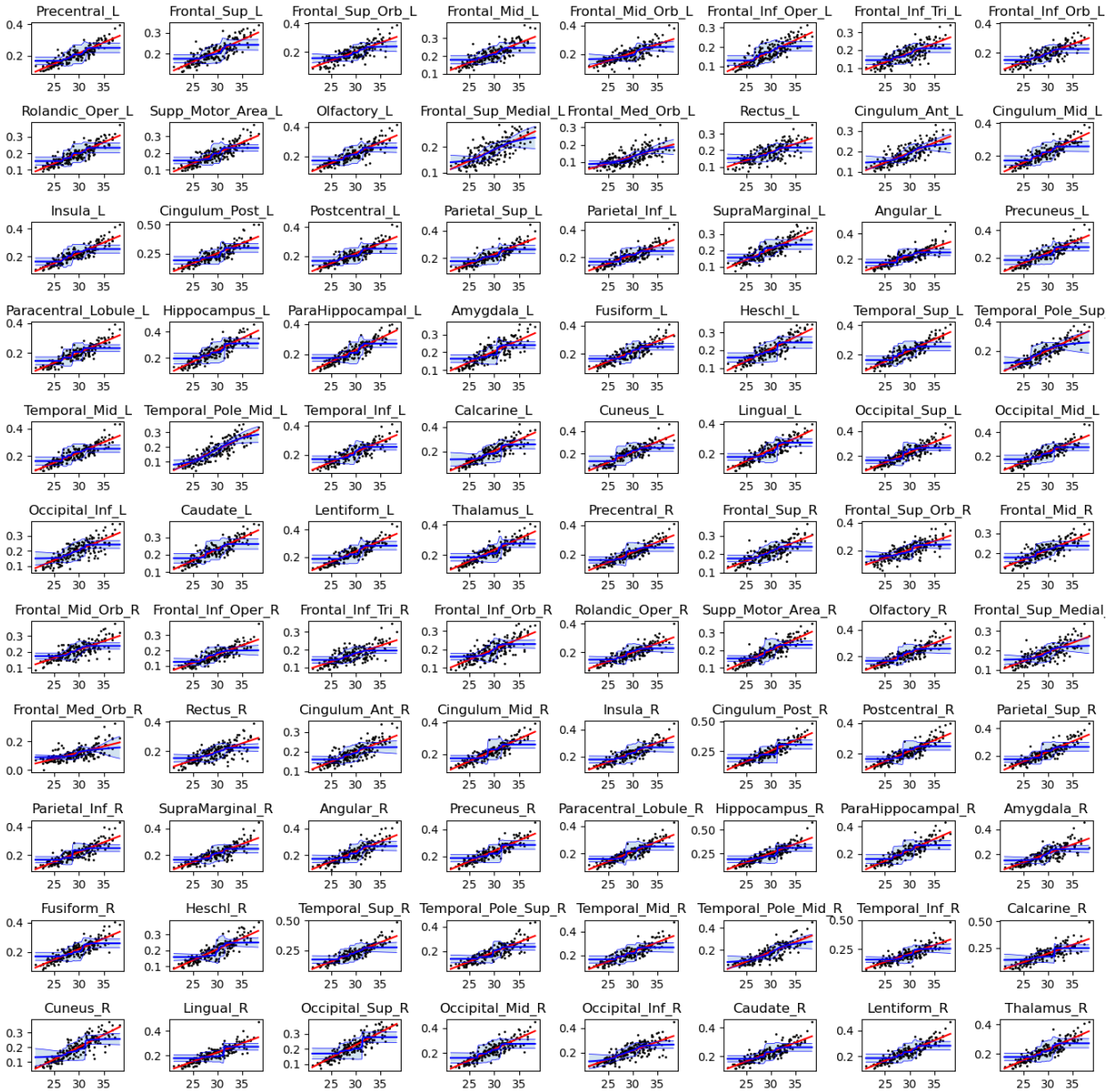

Figure 5: Connection strength for each of the 88 brain nodes as a function of gestational age. The black points represent data for individual fetuses. The red line is the linear fit. The blue lines and shade show the mean $\pm$ two standard deviations for the sigmoid fit.

parameter k in Equation (1), and found significantly steeper slopes in the left hemisphere compared to the right ($p = 10^{-5}$). However, within each hemisphere, there were no statistically significant differences in either the timing or the rate of nodal growth across different brain lobes. These results suggest that while hemispheric asymmetries in the dynamics of connectivity maturation do exist, particularly a slightly earlier and more rapid increase in the left hemisphere, the broader developmental trajectory remains well-synchronized across brain regions. The tight clustering of inflection points around 27.7–30.5 weeks likely marks a critical window of structural reorganization and accelerated white matter development during late gestation.

We further investigated how the strength of individual connections between brain regions evolved over

gestation by analyzing the temporal changes in edge strength. To assess the reproducibility of these developmental trends, we employed a robust resampling strategy. Specifically, for each network edge, we randomly selected 75% of the subjects without replacement and tested for a statistically significant linear association between edge strength and gestational age. This procedure was repeated 100 times per edge, and for each repetition, we recorded whether the edge exhibited a significant change. As shown in Figure 6, we summarized the results by calculating the percentage of repetitions in which each edge showed a significant association. To ensure high robustness, we retained only those edges that were significant in at least 95% of the repetitions. Based on this criterion, 162 edges demonstrated a consistent increase in strength over gestation, while 12 showed a consistent decrease. The strengthening edges encompassed both short-range and long-range connections, linking neighboring regions within lobes as well as distant regions across lobes and hemispheres. Notably, robust increases were observed in connections involving the anterior, middle, and posterior cingulate gyri, as well as in interhemispheric connections between the hippocampi. In contrast, the few connections that weakened with gestational age were primarily interhemispheric, including those linking the postcentral gyri, superior parietal lobules, and inferior parietal lobules in the parietal lobe, as well as the superior and medial frontal gyri in the frontal lobe. These findings suggest that while most structural connections strengthen during late gestation, a small subset of connections may be selectively pruned or refined as part of the maturation process.

3.1.3 Network hubs across the gestation

Finally, we identified the hubs of the structural connectome across gestational ages, using three complementary centrality metrics: (1) Degree centrality, which reflects the total connection strength of a node and captures its local importance; (2) Betweenness centrality [100], which quantifies the extent to which a node lies on the shortest paths between other node pairs, indicating its role as a connector or bridge; and (3) Eigenvector centrality [101], which measures a node's influence based on the importance of its neighbors and captures global network prominence. While degree centrality is inherently a local measure, both betweenness and eigenvector centrality capture global aspects of the network.

Figure 7 illustrates the distribution of network hubs at four gestational ages, based on eigenvector centrality. Several brain regions consistently emerged as hubs across most gestational weeks (22–37 weeks), including the precentral gyrus, superior and middle frontal gyri, precuneus, lentiform, and thalamus. Some regions showed increasing prominence with gestational age, notably the supplementary motor area, medial portion of the superior frontal gyrus, and insula. Conversely, a few regions, such as the middle temporal gyrus and inferior temporal gyrus, exhibited a decline in hub status over time, although they remained strongly connected.

Overall, there was substantial concordance among the three centrality measures, though some differences were observed. When defined by degree and betweenness centrality, the middle frontal gyrus and inferior temporal gyrus appeared less prominent, while the angular gyrus, fusiform gyrus, superior parietal lobule, and inferior parietal lobule emerged as more prominent hubs under these criteria.

Our findings broadly align with previous studies on structural connectome hubs in the human brain. In adults, commonly reported hub regions include the precuneus, superior frontal and superior parietal cortices, anterior and posterior cingulate cortex, insular cortex, temporal cortex, lentiform/putamen, thalamus, and hippocampus [102–108]. Several studies have also examined hub development in neonates and infants, often using functional MRI–based connectomes [57,109–111]. Reported structural hubs in neonates include the dorsal and medial frontal cortex, parietal cortex, precuneus, hippocampus, insula, and anterior cingulate cortex [7, 112, 113]. Functional hubs during the fetal and neonatal periods have been reported to include the cingulate cortex, precentral and postcentral gyri, superior parietal lobule, cerebellum, angular gyrus, fusiform gyrus, insula, and association cortices near the fusiform facial area and Wernicke's area [55, 57, 109, 111, 114–117]. The considerable overlap between hubs identified in our study and those reported in the literature lends support to the biological plausibility and generalizability of our findings. Notably, however, we did not identify the hippocampus or the cingulate cortex as major hubs, despite their frequent appearance as hubs in prior studies. These discrepancies may reflect differences in imaging modality, gestational age range, or methodological approach, including the definition of hub metrics and tractography techniques. In fetal imaging, in particular, there is a lack of standard computational methods, and difference in definitions of the extent of different cortical regions can lead to different results in

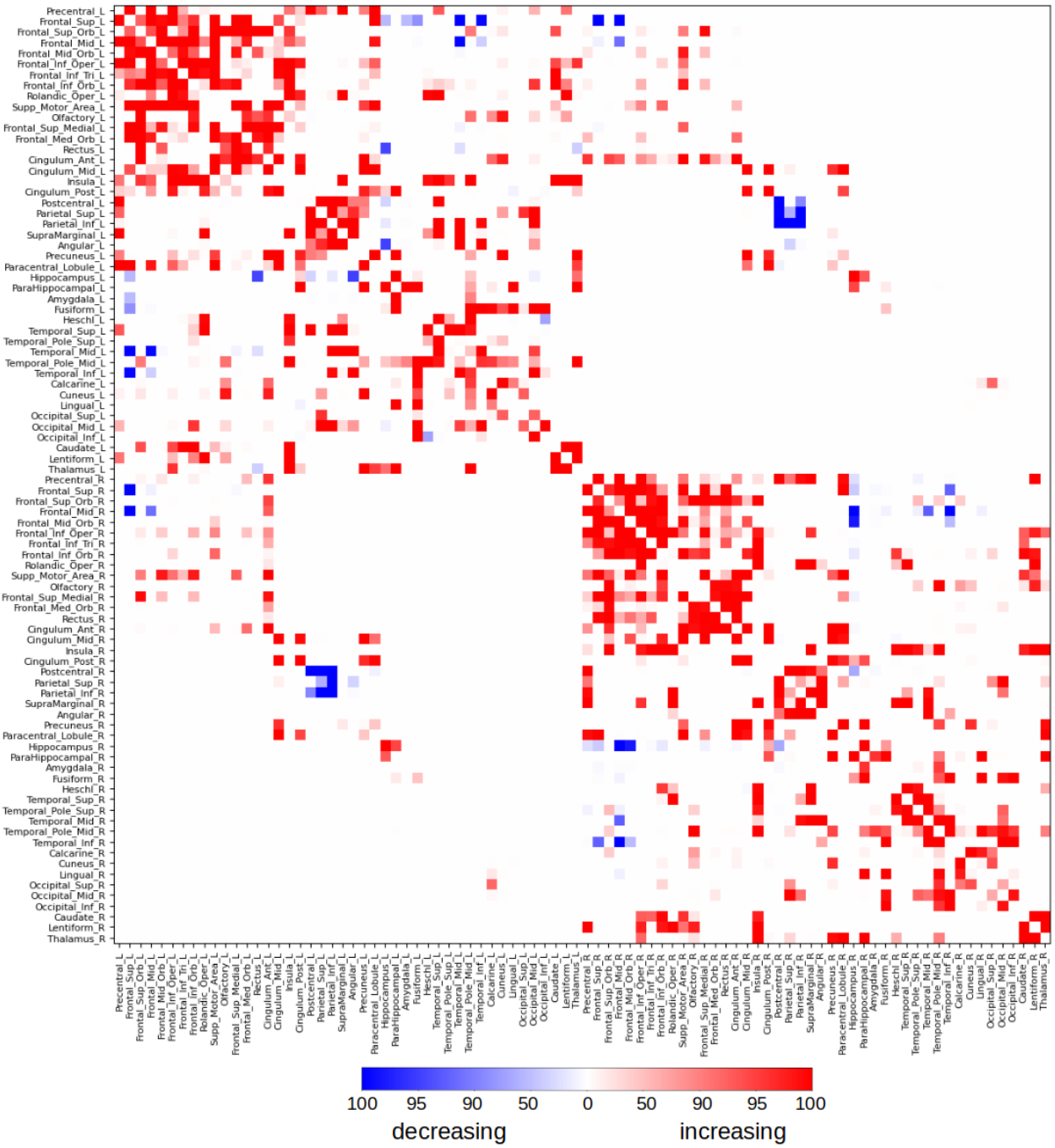

Figure 6: Change in the edge connection strength, i.e., the strength of connection between pairs of nodes, as a function of gestational age. We randomly selected 75% of the subjects and determined if there was a significant linear relation between the edge strength and gestational age. We repeated this 100 times for each edge. This figures shows the percentage of times the connection showed a significant increase (red) or decrease (blue) with gestational age.

determination of structural connectivity hubs.

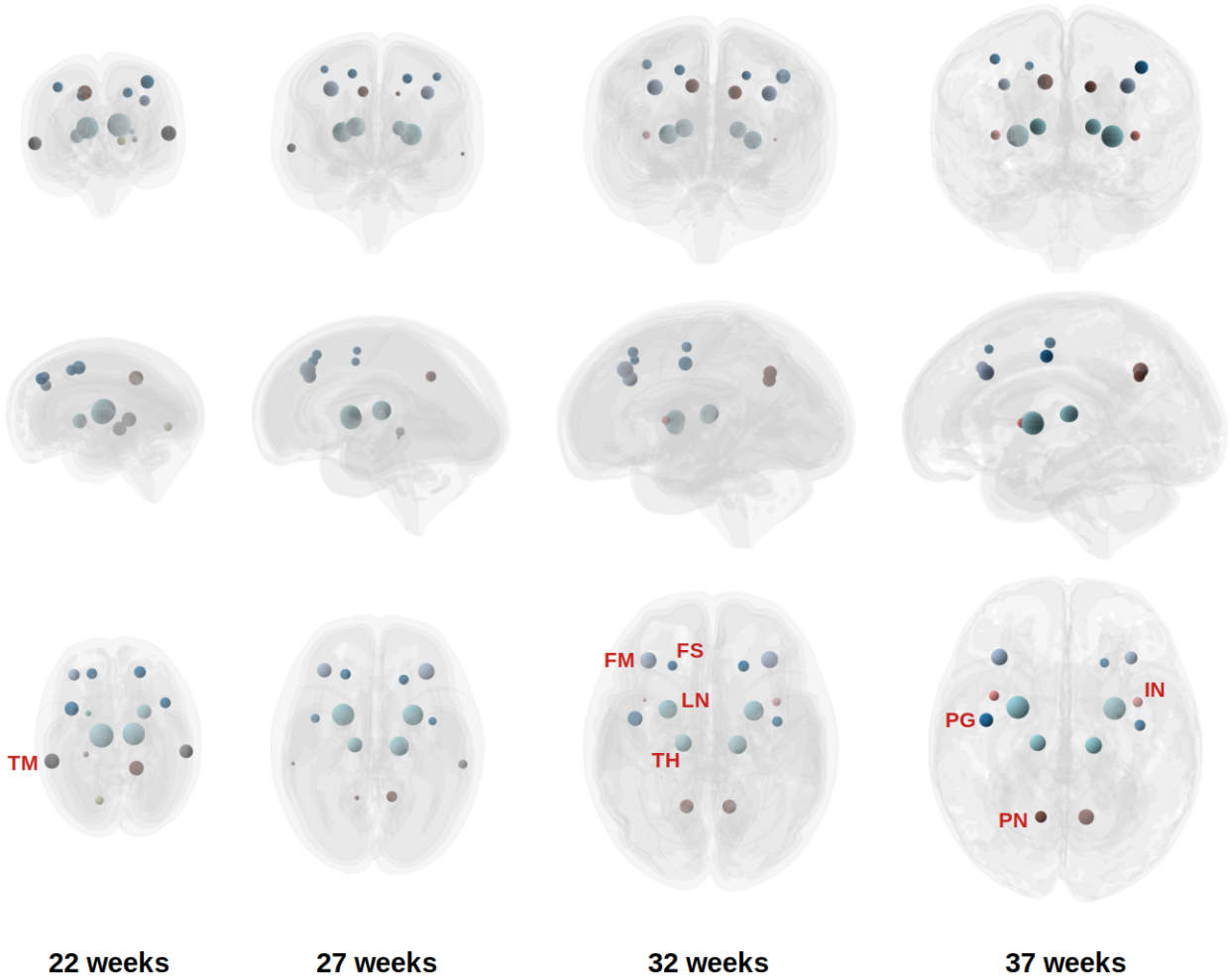

Figure 7: Network hubs identified on individual fetuses, averaged across all fetuses at each gestational week. The size of the sphere is proportional to the node strength for each hub. FS: Frontal superior gyrus; FM: Frontal middle gyrus; IN: Insula; LN: Lentiform; PN: Precuneus; PG: Precentral gyrus; TH: Thalamus; TM: Middle temporal gyrus.

3.2 Age-specific Connectome Templates

3.2.1 Comparison of different template reconstruction methods

Figure 8 presents the age-specific connectome templates for gestational weeks 22 to 37, generated using the proposed connectome aggregation method described in Section 2.4.1. For comparison, Figure 9 displays the corresponding templates constructed via image–space averaging, as detailed in Section 2.4.2. Both approaches yield connectomes that demonstrate a consistent increase in connection strength over gestation – within individual brain lobes, across different lobes, and between hemispheres. While the overall topological trends are broadly similar between the two methods, the templates derived from image–space averaging tend to show stronger inter-hemispheric connections. This is likely due to the spatial smoothing effect inherent in voxel-wise averaging across multiple subjects.

To quantitatively evaluate the performance of these methods, we compared the resulting templates to the individual connectomes of age-matched fetuses. Table 1 summarizes this comparison, which also includes the baseline method of distance-preserved averaging of connectomes [90]. The results for consensus-based thresholding were largely similar to distance-preserved averaging and, hence, are omitted from this table.

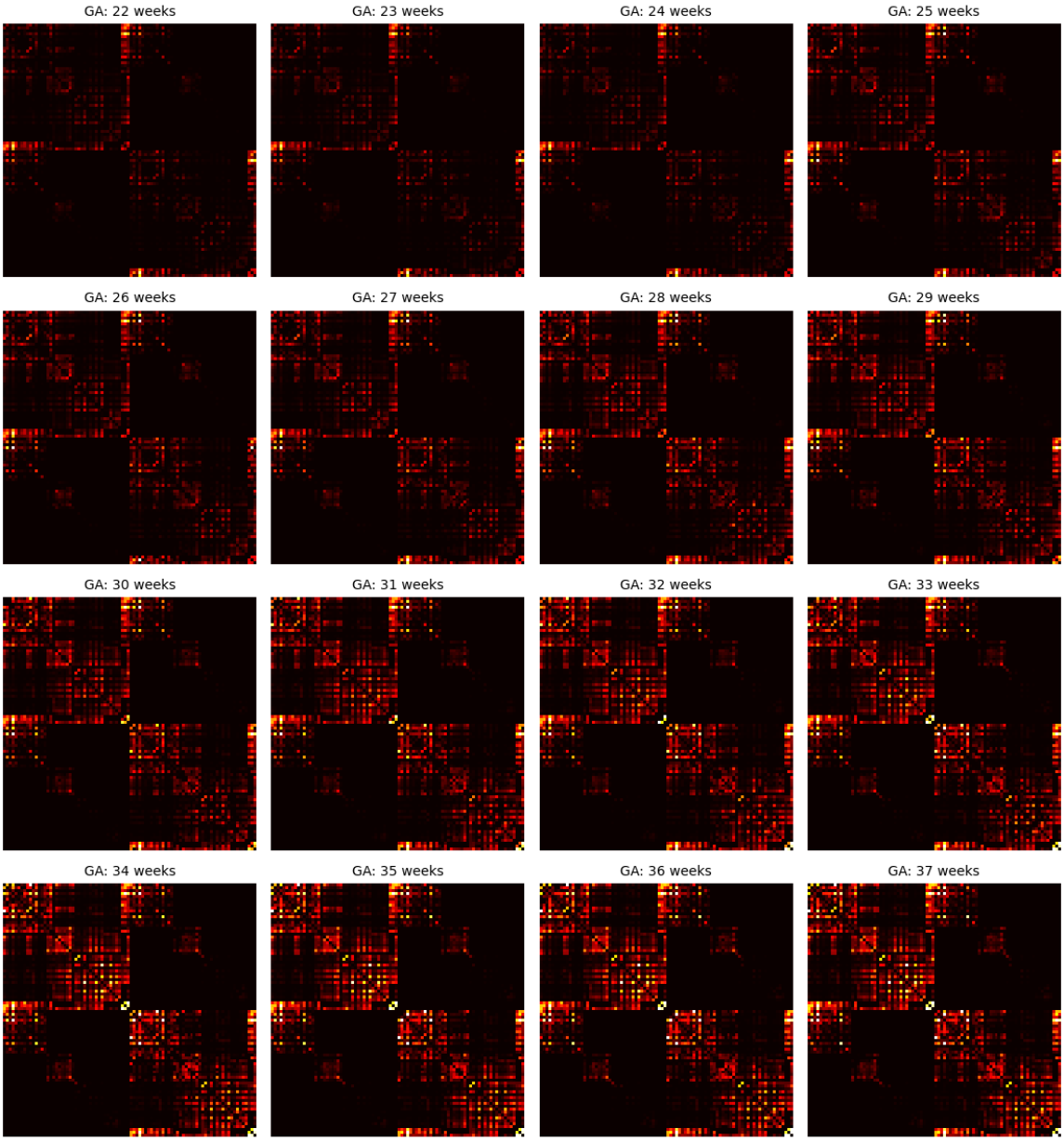

Figure 8: Connectome templates computed for every gestational age between 22 and 37 weeks with the connectome aggregation method proposed in Section 2.4.1.

For each template, we measured the difference in several key graph–theoretical metrics including global efficiency (GE), local efficiency (LE), characteristic path length (CPL), and total network strength, between the template and the corresponding individual connectomes. Across all metrics, the connectome aggregation method yielded templates that more closely resembled individual subject connectomes. Figure 4 shows a visual representation of these metrics.

We also evaluated the ability of each connectome template to capture age-related patterns using classification experiments. First, a nearest-neighbor classifier based on graph edit distance (GED) was used to predict the gestational age. Templates constructed via connectome aggregation achieved the lowest prediction error (0.98 ± 0.95 weeks), substantially outperforming both image–space averaging and element–wise averaging, which yielded errors greater than 2 weeks. Next, we implemented a more sophisticated classi-

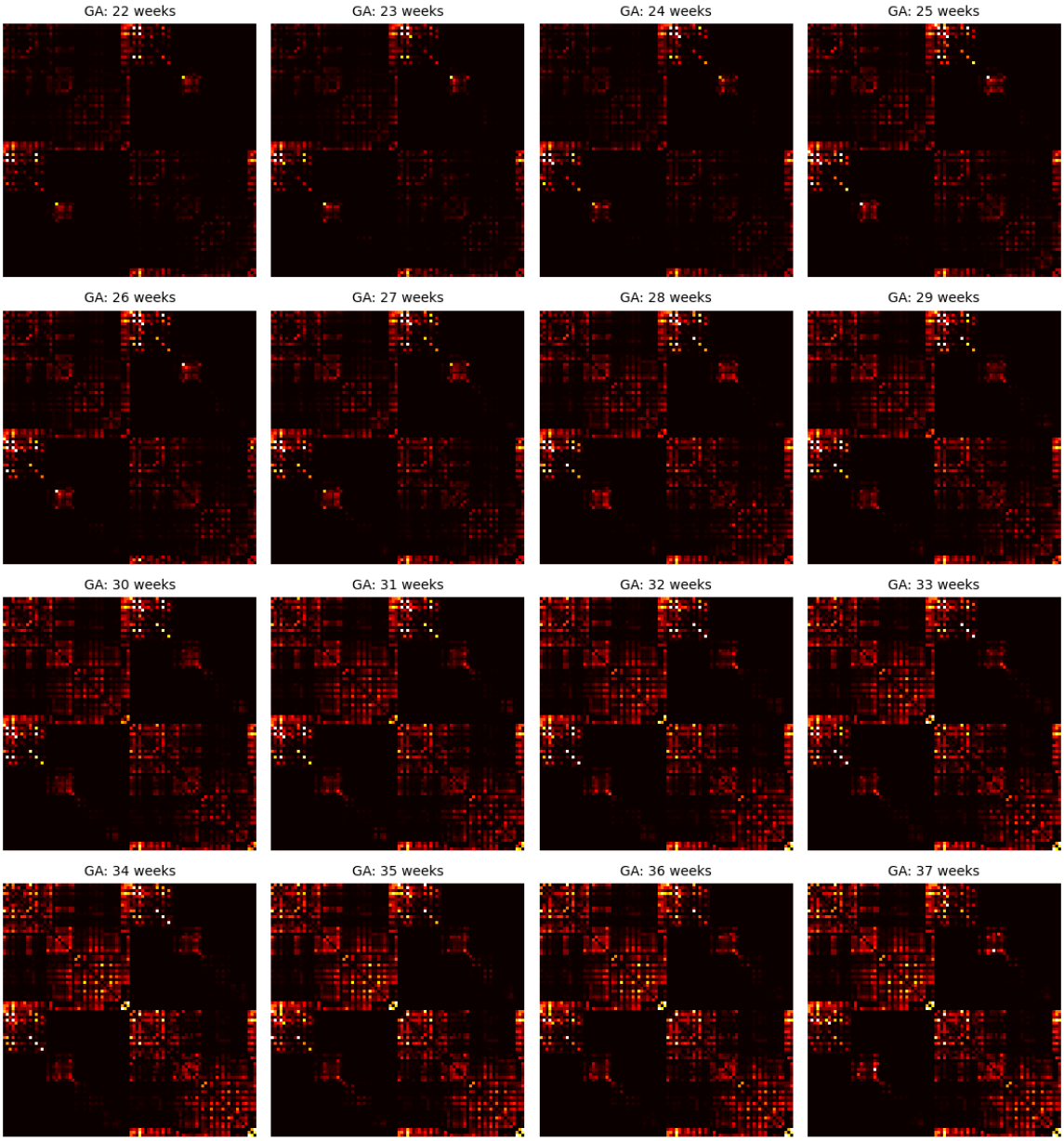

Figure 9: Connectome templates computed for every gestational week via data averaging in the image space described in Section 2.4.2.

fication framework based on the method in [98], described in Section 2.4. This method achieved an error of 0.90 weeks with the connectome aggregation templates, outperforming the other two methods (1.44 and 1.46 weeks, respectively). All results were validated using ten-fold cross-validation.

Finally, we assessed how well each method preserved the location of high-centrality nodes (i.e., hubs). For each gestational age, we identified the top 10 hubs in individual fetuses and their corresponding templates, and calculated the percentage of overlap. As shown in Table 1, the connectome aggregation–based templates had the highest agreement with the individual–level hubs (83% overlap), followed by image–space averaging (80%), and distance-preserved averaging (72%). These results indicate that connectome aggregation not only preserves overall network topology but also retains region–specific nodal prominence better than the other methods.

Table 1: Quantitative comparison of the connectome templates computed using different methods. The first four rows show the difference in the connectivity metrics between the individual subjects and their age–matched connectome templates. The next two rows show the accuracy of predicting the age of an individual fetus based on the similarity of his/her connectome with the age–specific connectome templates. More specifically, these two rows show the error (in weeks) in the predicted age of individual fetuses based on the similarity to the connectome templates. The last row shows the overlap of the 10 top hubs between each fetus and its age–matched connectome.

	Connectome aggregation method	Data averaging in the image space	Distance-preserved averaging [90]
GE	$\mathbf{0.240 \pm 0.207}$	0.375 ± 0.422	0.352 ± 0.228
LE	$\mathbf{0.039 \pm 0.029}$	0.058 ± 0.036	0.040 ± 0.037
CPL	$\mathbf{246 \pm 228}$	254 ± 214	256 ± 126
Network strength	$\mathbf{6.63 \pm 6.21}$	8.05 ± 6.83	8.38 ± 6.40
Age prediction error (in weeks), computed using on a nearest-neighbor classifier based on graph edit distance (GED)	$\mathbf{0.98 \pm 0.95}$	2.01 ± 1.39	2.77 ± 1.45
Age prediction error (in weeks), computed using a support vector machine classifier as in [98]	$\mathbf{0.90 \pm 0.81}$	1.44 ± 1.37	1.46 ± 1.85
Hub overlap	$\mathbf{0.83 \pm 0.08}$	0.80 ± 0.06	0.72 ± 0.07

3.2.2 Analysis of spatiotemporal trends based on the connectome templates

As summarized in Table 1 and illustrated in Figure 4, the connectome templates reconstructed using the connectome aggregation method outperformed those generated by alternative approaches in preserving key network characteristics. These high–fidelity templates were therefore used to analyze the developmental evolution of structural connectivity. Figure 10 presents four sets of plots illustrating the temporal dynamics of connectivity across different brain regions computed using these templates. Consistent with these visualizations and the connectome matrices shown in Figure 8, the fetal brain undergoes marked and progressive changes in structural connectivity between 22 and 37 gestational weeks.

The developmental trajectories are largely smooth and continuous, without any abrupt transitions. Nonetheless, for interpretability, we divided this interval into five approximately equal sub-periods, each capturing key developmental transitions during this critical stage of neurodevelopment.

Stage 1: 21–23 gestational weeks. At this early stage, global connectivity remains weak. Subcortical–cortical connections begin to emerge, particularly those linking the thalamus and lentiform nuclei to the developing frontal and parietal cortices. The corpus callosum is present but immature. Anatomically, the genu (the anterior portion of the corpus callosum) is among the first to form, allowing interhemispheric connection between homologous frontal areas. Likewise, the body of the corpus callosum begins to connect bilateral frontal and parietal lobes. Cortico–cortical connectivity within and between the lobes remains sparse, and although tractography recovers many intra–hemispheric association streamlines, their estimated weights based on fiber bundle capacity are negligible, reflecting immature or still-developing pathways.

Stage 2: 24–26 gestational weeks. This stage marks an increase in the strength of association pathways. Notably, intra-hemispheric connections between frontal and parietal lobes and between frontal and temporal lobes experience strengthening. The splenium of the corpus callosum, which connects the occipital lobes across hemispheres, begins to mature during this window, though these interhemispheric occipital connections remain weaker than their frontal and parietal counterparts. Thalamocortical projections to early visual areas such as the calcarine cortex, cuneus, and lingual gyrus also emerge, marking the onset of organized input to the occipital lobe. This can be seen in the plots as the early rise in thalamus–occipital connectivity.

Stage 3: 27–29 gestational weeks. This period is characterized by a consistent increase in the strength of nearly all connections, with several connections showing more pronounced acceleration. These include

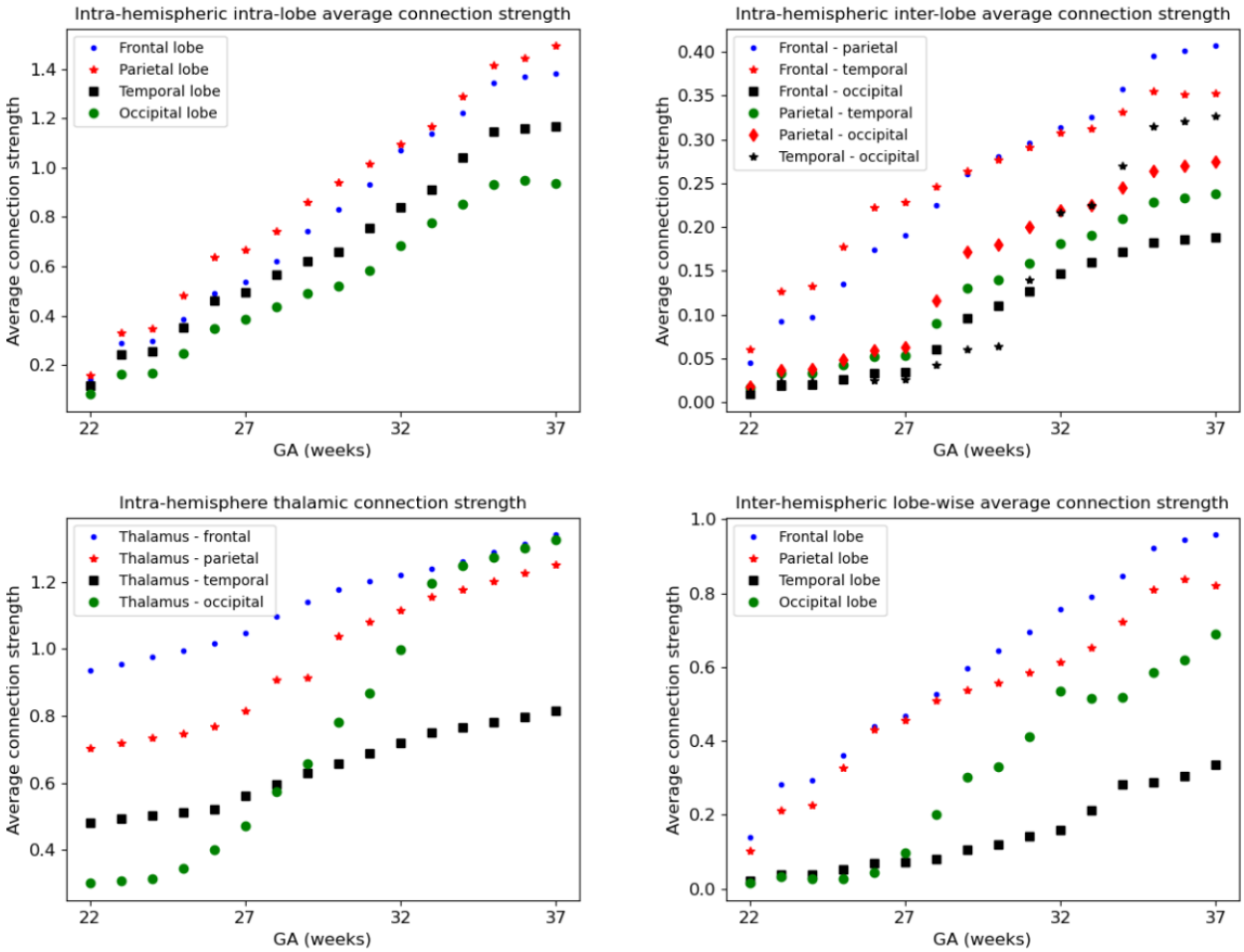

Figure 10: Development of structural connectivity across different brain regions computed using the connectome templates constructed with connectome aggregation method.

inter-hemispheric connections between the occipital lobes as well as the connections of occipital lobes to the thalami. Long-range intra-hemispheric association pathways also become more prominent, particularly those linking the occipital lobe to temporal and parietal regions. These maturing pathways form the anatomical substrate for higher cognitive and sensory integration processes that will support functions such as language, attention, and memory. Thalamocortical pathways continue to refine, particularly those targeting sensory and association cortices, contributing to the emerging coordination of large-scale brain networks.

Stage 4: 30–32 gestational weeks. Connectivity continues to strengthen globally, but several regional developments stand out. Interhemispheric temporal lobe connections, while still on average less strong than those of the frontal and parietal lobes, show signs of growth. Interhemispheric integration in the occipital lobe accelerates further as the splenium of the corpus callosum matures. Inter-lobe connections between the occipital and temporal lobes show a highly accelerated pace, much faster than all other intra-hemispheric inter-lobe connections at this stage, suggesting growing interdependence between visual and auditory/language processing areas. The insula, a key multisensory and salience–processing hub, exhibits increasing connectivity with multiple lobes, indicating its emerging role in integrating sensory, emotional, and cognitive information.

Stage 5: 33–37 gestational weeks. By late gestation, most major cortico-cortical association pathways – including those linking the temporal, occipital, and parietal lobes – are well established. Connectivity within the limbic system, particularly involving the amygdala and hippocampus, strengthens significantly,

especially in their projections to the cingulate and temporal cortices. While connection strength continues to increase both within and across lobes and hemispheres, the rate of change slows down in some pathways. This may suggest that the overall scaffold of the neonatal connectome is nearing completion by term-equivalent age. Postnatal development will likely involve fine-tuning processes such as myelination, pruning, and synaptic remodeling, building upon this robust structural backbone.

3.3 Reproducibility analysis

We evaluated the reproducibility of the reconstructed structural connectomes by assessing their consistency across independent subsets of dMRI measurements. The dMRI data for each fetus consisted of two shells: 46 measurements at $b = 400$ and 80 measurements at $b = 1000$. For each shell, we divided the measurements into two non-overlapping halves and reconstructed a separate connectome from each subset. Denoting the connectomes reconstructed for fetus i from the two subsets as C_i^A and C_i^B, we computed the graph edit distance between them to quantify intra-subject variability. As a reference, we also computed inter-subject GEDs by comparing C_i^A to C_j^A and C_i^B to C_j^B for all $i \neq j$. Intra-subject GEDs were significantly lower than inter-subject GEDs, with mean values of 5038 ± 1745 and 13619 ± 2603, respectively. For all 198 fetuses, the two connectomes derived from the independent subsets of their data were more similar to each other than to the connectomes of any other subject. This result demonstrates strong reproducibility of individual–specific structural connectivity profiles.

In addition, we computed several graph-theoretical metrics – SWI, CPL, GE, LE, CC – from each connectome derived from the two measurement subsets. We then fitted linear models to assess how each metric varied with gestational age, separately for each subset. The resulting regression models showed no significant differences in slope or intercept across the two data halves for any metric $p > 0.05$, further confirming the robustness and reproducibility of the estimated connectomes and the derived network properties.

4 Conclusions

To the best of our knowledge, this study represents the largest investigation of fetal brain structural connectivity using diffusion MRI. Analysis of connectivity metrics—including CPL, GE, CC, and LE—revealed a monotonic increase in the modular integration and segregation of structural brain networks during this period. We also observed a stable small-world configuration across gestational ages 22 to 37 weeks. The strength of connections for all 88 nodes examined increased as a function of gestational age. Fitting a sigmoid function to these data identified inflection points between 27.7 and 30.5 weeks, marking the period of most rapid connectivity strengthening. This window overlaps with the 29–31-week period reported as critical in a recent study of fetal functional connectivity [87], which found sharp increases in thalamocortical and cortico–cortical functional connectivity. Other studies of white-matter maturation based on FA and MD have suggested similar critical windows [44, 118]. For example, an analysis of 34 white-matter tracts reported turning points for both FA and MD between 27 and 32 weeks [118]. Taken together, our results further support the importance of this developmental interval in the formation of brain networks in utero.

A technical contribution of this work is the development of new methods for constructing connectome templates that characterize typical structural network development during the fetal period. Our evaluations showed that the proposed approach based on aggregating individual connectomes outperformed an alternative method that relied on precise spatiotemporal alignment and averaging of imaging data. The connectome-wise averaging approach produced templates that closely resembled the connectomes of age-matched fetuses in terms of connectivity metrics and hub distribution. In contrast, averaging in image space—despite its sophistication—yielded connectomes that deviated from those of individual subjects. This deviation likely reflects preferential weakening of some connections and strengthening of others as a consequence of data averaging in the image domain, as implemented here. Our image-space averaging method, described in Section 2.4.2 and Figure 1, closely follows approaches used in many prior fetal imaging studies [43, 94, 118, 119]. Therefore, our findings suggest that these widely used methods for constructing fetal brain templates do not preserve individual-level connectome features, although they may remain suitable for other purposes such as characterizing specific brain regions or local tissue and microstructural development.

Using the connectome templates generated through connectome aggregation, we characterized spatiotemporal trends in fetal brain connectivity between 22 and 37 gestational weeks. Although the developmental trajectory appeared largely continuous, we divided this period into five sub-phases to highlight key transitions in structural maturation. Around 22 weeks, thalamocortical connections are relatively strong, whereas cortico–cortical connections—both within and between hemispheres—remain immature. By 37 weeks, dense and symmetric connectivity is evident within individual lobes, across lobes, and between homologous regions across hemispheres. Each developmental stage exhibited distinct patterns of accelerated growth in specific pathways, including thalamocortical visual projections, intra- and inter-hemispheric occipital–temporal associations, and the emergence of insular hub connectivity, reflecting the sequential establishment of large-scale functional systems during gestation.

Although the reproducibility of tractography and quantitative connectomics remains an active area of investigation, our reproducibility analysis produced encouraging results. Connectomes reconstructed from two non-overlapping subsets of dMRI measurements for each fetus were substantially more similar to one another than to those of any other subject, demonstrating strong individual specificity. Bootstrapped assessments of nodal and edge-wise connectivity further confirmed statistically robust and reproducible developmental patterns, as shown in Figures 5 and 6. Moreover, the ability of the age-specific connectome templates to predict gestational age with an average error of less than one week suggests that the structural connectome captures meaningful and temporally specific developmental signatures. Taken together, these findings indicate that—despite inherent limitations in fetal dMRI and tractography—current methodologies can capture individualized profiles of fetal brain connectivity. As such, structural connectomics may provide a valuable framework for studying both normative and atypical patterns of prenatal brain development.

Despite broad agreement with the existing literature, several differences between our findings and prior studies are noteworthy. For example, the SWI values observed in our study were lower and more stable than those previously reported, where values substantially greater than one and sharp age-related increases have been described [55, 58, 60, 120–122]. Similarly, although our hub analysis identified regions consistent with earlier structural and functional studies—including the precuneus, thalamus, lentiform nucleus, and medial frontal cortex—we did not consistently identify the hippocampus or cingulate cortex as major hubs. Several factors may account for these discrepancies. Different definitions of the small-world index exist, and not all prior studies clearly specify which definition they used [123–125]. More importantly, many earlier works employed deterministic tractography and surrogate connectivity measures such as streamline count or FA [55, 58, 60, 126, 127], whereas our analysis relied on anatomically constrained tractography tailored to fetal anatomy [78] and a biologically grounded measure of connection weight based on fiber bundle capacity [9, 85]. Finally, the size and quality of the dataset used here far exceed those of prior fetal studies, enabling more robust and generalizable conclusions. For these reasons, we believe our findings provide new insights that may help reinterpret results from earlier work in this area.

Acknowledgments

This research was supported in part by the National Institute of Neurological Disorders and Stroke and Eunice Kennedy Shriver National Institute of Child Health and Human Development of the National Institutes of Health (NIH) under award numbers R01HD110772, R01NS128281, R01EB036945, and R01LM013608. The content of this publication is solely the responsibility of the authors and does not necessarily represent the official views of the NIH. The dHCP data were provided by the developing Human Connectome Project, KCL-Imperial-Oxford Consortium funded by the European Research Council under the European Union Seventh Framework Programme (FP/2007-2013) / ERC Grant Agreement no. [319456]. We are grateful to the families who generously supported this trial.

References

[1] Sebastian Seung. *Connectome: How the brain's wiring makes us who we are*. HMH, 2012.

[2] Olaf Sporns, Giulio Tononi, and Rolf Kötter. The human connectome: a structural description of the human brain. *PLoS computational biology*, 1(4):e42, 2005.

[3] Guusje Collin and Martijn P Van Den Heuvel. The ontogeny of the human connectome: development and dynamic changes of brain connectivity across the life span. *The Neuroscientist*, 19(6):616–628, 2013.

[4] Edward T Bullmore and Danielle S Bassett. Brain graphs: graphical models of the human brain connectome. *Annual review of clinical psychology*, 7:113–140, 2011.

[5] Yonggang Shi and Arthur W Toga. Connectome imaging for mapping human brain pathways. *Molecular psychiatry*, 22(9):1230–1240, 2017.

[6] Olaf Sporns. *Networks of the Brain*. MIT press, 2016.

[7] O Tymofiyeva, CP Hess, D Xu, and AJ Barkovich. Structural mri connectome in development: challenges of the changing brain. *The British journal of radiology*, 87(1039):20140086, 2014.

[8] PM Rossini, Riccardo Di Iorio, M Bentivoglio, G Bertini, F Ferreri, C Gerloff, RJ Ilmoniemi, F Miraglia, MA Nitsche, F Pestilli, et al. Methods for analysis of brain connectivity: An ifcn-sponsored review. *Clinical Neurophysiology*, 130(10):1833–1858, 2019.

[9] Robert E Smith, David Raffelt, J-Donald Tournier, and Alan Connelly. Quantitative streamlines tractography: methods and inter-subject normalisation. *Aperture Neuro*, pages 1–25, 2022.

[10] Fan Zhang, Alessandro Daducci, Yong He, Simona Schiavi, Caio Seguin, Robert Smith, Chun-Hung Yeh, Tengda Zhao, and Lauren J O'Donnell. Quantitative mapping of the brain's structural connectivity using diffusion mri tractography: a review. *NeuroImage*, page 118870, 2022.

[11] Stamatios N Sotiropoulos and Andrew Zalesky. Building connectomes using diffusion mri: why, how and but. *NMR in Biomedicine*, 32(4):e3752, 2019.

[12] Mikail Rubinov and Olaf Sporns. Complex network measures of brain connectivity: uses and interpretations. *Neuroimage*, 52(3):1059–1069, 2010.

[13] Shouliang Qi, Stephan Meesters, Klaas Nicolay, Bart M ter Haar Romeny, and Pauly Ossenblok. The influence of construction methodology on structural brain network measures: A review. *Journal of neuroscience methods*, 253:170–182, 2015.

[14] Derek K Jones, Thomas R Knösche, and Robert Turner. White matter integrity, fiber count, and other fallacies: the do's and don'ts of diffusion mri. *Neuroimage*, 73:239–254, 2013.

[15] Alex Fornito, Andrew Zalesky, and Michael Breakspear. Graph analysis of the human connectome: promise, progress, and pitfalls. *Neuroimage*, 80:426–444, 2013.

[16] Derek K Jones. Challenges and limitations of quantifying brain connectivity in vivo with diffusion mri. *Imaging in Medicine*, 2(3):341, 2010.

[17] Mark Drakesmith, Karen Caeyenberghs, A Dutt, G Lewis, AS David, and Derek K Jones. Overcoming the effects of false positives and threshold bias in graph theoretical analyses of neuroimaging data. *Neuroimage*, 118:313–333, 2015.

[18] Joseph Yuan-Mou Yang, Chun-Hung Yeh, Cyril Poupon, and Fernando Calamante. Diffusion mri tractography for neurosurgery: the basics, current state, technical reliability and challenges. *Physics in Medicine & Biology*, 66(15):15TR01, 2021.

[19] Yaniv Assaf and Ofer Pasternak. Diffusion tensor imaging (dti)-based white matter mapping in brain research: a review. *Journal of molecular neuroscience*, 34(1):51–61, 2008.

[20] Walid I Essayed, Fan Zhang, Prashin Unadkat, G Rees Cosgrove, Alexandra J Golby, and Lauren J O'Donnell. White matter tractography for neurosurgical planning: A topography-based review of the current state of the art. *NeuroImage: Clinical*, 15:659–672, 2017.

[21] Olga Ciccarelli, Marco Catani, Heidi Johansen-Berg, Chris Clark, and Alan Thompson. Diffusion-based tractography in neurological disorders: concepts, applications, and future developments. *The Lancet Neurology*, 7(8):715–727, 2008.

[22] Cibu Thomas, Q Ye Frank, M Okan Irfanoglu, Pooja Modi, Kadharbatcha S Saleem, David A Leopold, and Carlo Pierpaoli. Anatomical accuracy of brain connections derived from diffusion mri tractography is inherently limited. *Proceedings of the National Academy of Sciences*, 111(46):16574–16579, 2014.

[23] Alessandra Griffa, Philipp S Baumann, Jean-Philippe Thiran, and Patric Hagmann. Structural connectomics in brain diseases. *Neuroimage*, 80:515–526, 2013.

[24] Chun-Yi Lo, Pei-Ning Wang, Kun-Hsien Chou, Jinhui Wang, Yong He, and Ching-Po Lin. Diffusion tensor tractography reveals abnormal topological organization in structural cortical networks in alzheimer's disease. *Journal of Neuroscience*, 30(50):16876–16885, 2010.

[25] Danielle S Bassett and Edward T Bullmore. Human brain networks in health and disease. *Current opinion in neurology*, 22(4):340, 2009.

[26] Ashish Raj, Amy Kuceyeski, and Michael Weiner. A network diffusion model of disease progression in dementia. *Neuron*, 73(6):1204–1215, 2012.

[27] Qingjiu Cao, Ni Shu, Li An, Peng Wang, Li Sun, Ming-Rui Xia, Jin-Hui Wang, Gao-Lang Gong, Yu-Feng Zang, Yu-Feng Wang, et al. Probabilistic diffusion tractography and graph theory analysis reveal abnormal white matter structural connectivity networks in drug-naive boys with attention deficit/hyperactivity disorder. *Journal of Neuroscience*, 33(26):10676–10687, 2013.

[28] Soon-Beom Hong, Andrew Zalesky, Alex Fornito, Subin Park, Young-Hui Yang, Min-Hyeon Park, In-Chan Song, Chul-Ho Sohn, Min-Sup Shin, Bung-Nyun Kim, et al. Connectomic disturbances in attention-deficit/hyperactivity disorder: a whole-brain tractography analysis. *Biological psychiatry*, 76(8):656–663, 2014.

[29] Anne L Wheeler and Aristotle N Voineskos. A review of structural neuroimaging in schizophrenia: from connectivity to connectomics. *Frontiers in human neuroscience*, 8:653, 2014.

[30] David R Goldsmith, Courtney L Crooks, Elaine F Walker, and Robert O Cotes. An update on promising biomarkers in schizophrenia. *Focus*, 16(2):153–163, 2018.

[31] Emilia Sbardella, Francesca Tona, Nikolaos Petsas, and Patrizia Pantano. Dti measurements in multiple sclerosis: evaluation of brain damage and clinical implications. *Multiple sclerosis international*, 2013, 2013.

[32] Vinzenz Fleischer, Adriane Gröger, Nabin Koirala, Amgad Droby, Muthuraman Muthuraman, Pierre Kolber, Eva Reuter, Sven G Meuth, Frauke Zipp, and Sergiu Groppa. Increased structural white and grey matter network connectivity compensates for functional decline in early multiple sclerosis. *Multiple Sclerosis Journal*, 23(3):432–441, 2017.

[33] Tengda Zhao, Miao Cao, Haijing Niu, Xi-Nian Zuo, Alan Evans, Yong He, Qi Dong, and Ni Shu. Age-related changes in the topological organization of the white matter structural connectome across the human lifespan. *Human brain mapping*, 36(10):3777–3792, 2015.

[34] Wei Wen, Wanlin Zhu, Yong He, Nicole A Kochan, Simone Reppermund, Melissa J Slavin, Henry Brodaty, John Crawford, Aihua Xia, and Perminder Sachdev. Discrete neuroanatomical networks are associated with specific cognitive abilities in old age. *Journal of Neuroscience*, 31(4):1204–1212, 2011.

[35] Minhui Ouyang, Jessica Dubois, Qinlin Yu, Pratik Mukherjee, and Hao Huang. Delineation of early brain development from fetuses to infants with diffusion mri and beyond. *Neuroimage*, 185:836–850, 2019.

[36] Hao Huang, Jiangyang Zhang, Setsu Wakana, Weihong Zhang, Tianbo Ren, Linda J Richards, Paul Yarowsky, Pamela Donohue, Ernest Graham, Peter CM van Zijl, et al. White and gray matter development in human fetal, newborn and pediatric brains. *Neuroimage*, 33(1):27–38, 2006.

[37] Hao Huang, Rong Xue, Jiangyang Zhang, Tianbo Ren, Linda J Richards, Paul Yarowsky, Michael I Miller, and Susumu Mori. Anatomical characterization of human fetal brain development with diffusion tensor magnetic resonance imaging. *Journal of Neuroscience*, 29(13):4263–4273, 2009.

[38] András Jakab, Gregor Kasprian, Ernst Schwartz, Gerlinde Maria Gruber, Christian Mitter, Daniela Prayer, Veronika Schöpf, and Georg Langs. Disrupted developmental organization of the structural connectome in fetuses with corpus callosum agenesis. *Neuroimage*, 111:277–288, 2015.

[39] Jessica Dubois, Ghislaine Dehaene-Lambertz, Sofya Kulikova, Cyril Poupon, Petra S Hüppi, and Lucie Hertz-Pannier. The early development of brain white matter: a review of imaging studies in fetuses, newborns and infants. *Neuroscience*, 276:48–71, 2014.

[40] András Jakab, Ruth Tuura, Christian Kellenberger, and Ianina Scheer. In utero diffusion tensor imaging of the fetal brain: a reproducibility study. *NeuroImage: Clinical*, 15:601–612, 2017.

[41] Anqi Qiu, Susumu Mori, and Michael I Miller. Diffusion tensor imaging for understanding brain development in early life. *Annual review of psychology*, 66:853–876, 2015.

[42] Ruike Chen, Ruoke Zhao, Haotian Li, Xinyi Xu, Mingyang Li, Zhiyong Zhao, Cong Sun, Guangbin Wang, and Dan Wu. Development of the fetal brain corticocortical structural network during the second-to-third trimester based on diffusion mri. *Journal of Neuroscience*, 44(29), 2024.

[43] Shadab Khan, Lana Vasung, Bahram Marami, Caitlin K Rollins, Onur Afacan, Cynthia M Ortinau, Edward Yang, Simon K Warfield, and Ali Gholipour. Fetal brain growth portrayed by a spatiotemporal diffusion tensor mri atlas computed from in utero images. *NeuroImage*, 185:593–608, 2019.

[44] Siân Wilson, Maximilian Pietsch, Lucilio Cordero-Grande, Anthony N Price, Jana Hutter, Jiaxin Xiao, Laura McCabe, Mary A Rutherford, Emer J Hughes, Serena J Counsell, et al. Development of human white matter pathways in utero over the second and third trimester. *Proceedings of the National Academy of Sciences*, 118(20), 2021.

[45] Maximilian Pietsch, Daan Christiaens, Jana Hutter, Lucilio Cordero-Grande, Anthony N Price, Emer Hughes, A David Edwards, Joseph V Hajnal, Serena J Counsell, and J-Donald Tournier. A framework for multi-component analysis of diffusion mri data over the neonatal period. *Neuroimage*, 186:321–337, 2019.

[46] Petra S Hüppi and Jessica Dubois. Diffusion tensor imaging of brain development. In *Seminars in Fetal and Neonatal Medicine*, volume 11, pages 489–497. Elsevier, 2006.

[47] John C Silbereis, Sirisha Pochareddy, Ying Zhu, Mingfeng Li, and Nenad Sestan. The cellular and molecular landscapes of the developing human central nervous system. *Neuron*, 89(2):248–268, 2016.

[48] Ivica Kostović and Nataša Jovanov-Milošević. The development of cerebral connections during the first 20–45 weeks' gestation. *Seminars in Fetal and Neonatal Medicine*, 11(6):415–422, 2006.

[49] Shirley A Bayer and Joseph Altman. *The human brain during the second trimester*. CRC Press, 2005.

[50] Jeremy A Miller, Song-Lin Ding, Susan M Sunkin, Kimberly A Smith, Lydia Ng, Aaron Szafer, Amanda Ebbert, Zackery L Riley, Joshua J Royall, Kaylynn Aiona, et al. Transcriptional landscape of the prenatal human brain. *Nature*, 508(7495):199–206, 2014.

[51] Giorgio M Innocenti and David J Price. Exuberance in the development of cortical networks. *Nature Reviews Neuroscience*, 6(12):955–965, 2005.

[52] Elena Taverna, Magdalena Götz, and Wieland B Huttner. The cell biology of neurogenesis: toward an understanding of the development and evolution of the neocortex. *Annual review of cell and developmental biology*, 30:465–502, 2014.

[53] PILA Yakovlev. The myelogenetic cycles of regional maturation of the brain. *Regional development of the brain in early life*, pages 3–70, 1967.

[54] Igor Jakovcevski, Radmila Filipovic, Zhicheng Mo, Sonja Rakic, and Nada Zecevic. Oligodendrocyte development and the onset of myelination in the human fetal brain. *Frontiers in neuroanatomy*, 3:5, 2009.

[55] Martijn P Van Den Heuvel, Karina J Kersbergen, Marcel A De Reus, Kristin Keunen, René S Kahn, Floris Groenendaal, Linda S De Vries, and Manon JNL Benders. The neonatal connectome during preterm brain development. *Cerebral cortex*, 25(9):3000–3013, 2015.

[56] Emi Takahashi, Rebecca D Folkerth, Albert M Galaburda, and Patricia E Grant. Emerging cerebral connectivity in the human fetal brain: an mr tractography study. *Cerebral cortex*, 22(2):455–464, 2012.

[57] Miao Cao, Hao Huang, and Yong He. Developmental connectomics from infancy through early childhood. *Trends in neurosciences*, 40(8):494–506, 2017.

[58] Limei Song, Virendra Mishra, Minhui Ouyang, Qinmu Peng, Michelle Slinger, Shuwei Liu, and Hao Huang. Human fetal brain connectome: structural network development from middle fetal stage to birth. *Frontiers in neuroscience*, 11:561, 2017.

[59] Tengda Zhao, Virendra Mishra, Tina Jeon, Minhui Ouyang, Qinmu Peng, Lina Chalak, Jessica Lee Wisnowski, Roy Heyne, Nancy Rollins, Ni Shu, et al. Structural network maturation of the preterm human brain. *Neuroimage*, 185:699–710, 2019.

[60] Colin J Brown, Steven P Miller, Brian G Booth, Shawn Andrews, Vann Chau, Kenneth J Poskitt, and Ghassan Hamarneh. Structural network analysis of brain development in young preterm neonates. *Neuroimage*, 101:667–680, 2014.

[61] Elise Turk, Marion I Van Den Heuvel, Manon J Benders, Roel De Heus, Arie Franx, Janessa H Manning, Jasmine L Hect, Edgar Hernandez-Andrade, Sonia S Hassan, Roberto Romero, et al. Functional connectome of the fetal brain. *Journal of Neuroscience*, 39(49):9716–9724, 2019.

[62] Pew-Thian Yap, Yong Fan, Yasheng Chen, John H Gilmore, Weili Lin, and Dinggang Shen. Development trends of white matter connectivity in the first years of life. *PloS one*, 6(9):e24678, 2011.

[63] Yong Fan, Feng Shi, Jeffrey Keith Smith, Weili Lin, John H Gilmore, and Dinggang Shen. Brain anatomical networks in early human brain development. *Neuroimage*, 54(3):1862–1871, 2011.

[64] Mary T Donofrio, Catherine Limperopoulos, et al. Impact of congenital heart disease on fetal brain development and injury. *Current opinion in pediatrics*, 23(5):502–511, 2011.

[65] John Kylan Lynch. Epidemiology and classification of perinatal stroke. *Seminars in Fetal and Neonatal Medicine*, 14(5):245–249, 2009.

[66] Karen Markussen Linnet, Søren Dalsgaard, Carsten Obel, Kirsten Wisborg, Tine Brink Henriksen, Alina Rodriguez, Arto Kotimaa, Irma Moilanen, Per Hove Thomsen, Jørn Olsen, et al. Maternal lifestyle factors in pregnancy risk of attention deficit hyperactivity disorder and associated behaviors: review of the current evidence. *American Journal of Psychiatry*, 160(6):1028–1040, 2003.

[67] Joanna Maselko, Siham Sikander, Sonia Bhalotra, Omer Bangash, Nima Ganga, Satadru Mukherjee, Helen Egger, Lauren Franz, Amina Bibi, Rakhshanda Liaqat, et al. Effect of an early perinatal depression intervention on long-term child development outcomes: follow-up of the thinking healthy programme randomised controlled trial. *The Lancet Psychiatry*, 2(7):609–617, 2015.

[68] Alexandra Sawyer, Susan Ayers, and Helen Smith. Pre-and postnatal psychological wellbeing in africa: a systematic review. *Journal of affective disorders*, 123(1-3):17–29, 2010.

[69] Dennis K Kinney, Kerim M Munir, David J Crowley, and Andrea M Miller. Prenatal stress and risk for autism. *Neuroscience & Biobehavioral Reviews*, 32(8):1519–1532, 2008.

[70] Vincent J Schmithorst, Jodie K Votava-Smith, Nhu Tran, Richard Kim, Vince Lee, Rafael Ceschin, Hollie Lai, Jennifer A Johnson, Joan Sanchez De Toledo, Stefan Blüml, et al. Structural network topology correlates of microstructural brain dysmaturation in term infants with congenital heart disease. *Human brain mapping*, 39(11):4593–4610, 2018.

[71] Catherine Limperopoulos, Wayne Tworetzky, Doff B McElhinney, Jane W Newburger, David W Brown, Richard L Robertson Jr, Nicolas Guizard, Ellen McGrath, Judith Geva, David Annese, et al. Brain volume and metabolism in fetuses with congenital heart disease: evaluation with quantitative magnetic resonance imaging and spectroscopy. *Circulation*, 121(1):26–33, 2010.

[72] C Jaimes, V Rofeberg, C Stopp, CM Ortinau, A Gholipour, KG Friedman, W Tworetzky, J Estroff, JW Newburger, D Wypij, et al. Association of isolated congenital heart disease with fetal brain maturation. *American Journal of Neuroradiology*, 41(8):1525–1531, 2020.

[73] A Meoded, A Poretti, A Tekes, A Flammang, S Pryde, and TAGM Huisman. Prenatal mr diffusion tractography in a fetus with complete corpus callosum agenesis. *Neuropediatrics*, 42(03):122–123, 2011.

[74] Gregor Kasprian, Peter C Brugger, Veronika Schöpf, Christian Mitter, Michael Weber, Johannes A Hainfellner, and Daniela Prayer. Assessing prenatal white matter connectivity in commissural agenesis. *Brain*, 136(1):168–179, 2013.

[75] A-E Millischer, D Grevent, P Sonigo, N Bahi-Buisson, I Desguerre, H Mahallati, J-P Bault, T Quibel, S Couderc, M-L Moutard, et al. Feasibility and added value of fetal dti tractography in the evaluation of an isolated short corpus callosum: Preliminary results. *American Journal of Neuroradiology*, 43(1):132–138, 2022.

[76] Hao Huang. Delineating neural structures of developmental human brains with diffusion tensor imaging. *TheScientificWorldJOURNAL*, 10:135–144, 2010.

[77] Gang Xu, Emi Takahashi, Rebecca D Folkerth, Robin L Haynes, Joseph J Volpe, P Ellen Grant, and Hannah C Kinney. Radial coherence of diffusion tractography in the cerebral white matter of the human fetus: neuroanatomic insights. *Cerebral cortex*, 24(3):579–592, 2014.

[78] Camilo Calixto, Camilo Jaimes, Matheus D Soldatelli, Simon K Warfield, Ali Gholipour, and Davood Karimi. Anatomically constrained tractography of the fetal brain. *arXiv preprint arXiv:2403.02444*, 2024.

[79] Weide Liu, Camilo Calixto, Simon K Warfield, and Davood Karimi. Streamline tractography of the fetal brain in utero with machine learning. *Imaging Neuroscience*, 3:imag_a_00537, 2025.

[80] Daan Christiaens, Lucilio Cordero-Grande, Maximilian Pietsch, Jana Hutter, Anthony N Price, Emer J Hughes, Katy Vecchiato, Maria Deprez, A David Edwards, Joseph V Hajnal, et al. Scattered slice shard reconstruction for motion correction in multi-shell diffusion mri. *Neuroimage*, 225:117437, 2021.

[81] Ben Jeurissen, Jacques-Donald Tournier, Thijs Dhollander, Alan Connelly, and Jan Sijbers. Multi-tissue constrained spherical deconvolution for improved analysis of multi-shell diffusion mri data. *NeuroImage*, 103:411–426, 2014.

[82] J-Donald Tournier, Fernando Calamante, and Alan Connelly. Robust determination of the fibre orientation distribution in diffusion mri: non-negativity constrained super-resolved spherical deconvolution. *Neuroimage*, 35(4):1459–1472, 2007.

[83] Davood Karimi, Camilo Calixto Nunez, Haykel Snoussi, Maria Camila Cortes-Albornoz, Clemente Velasco-Annis, Caitlin Rollins, Camilo Jaimes, Ali Gholipour, and Simon K Warfield. Detailed delineation of the fetal brain in diffusion mri via multi-task learning. *bioRxiv*, pages 2024–08, 2024.

[84] J Donald Tournier, Fernando Calamante, Alan Connelly, et al. Improved probabilistic streamlines tractography by 2nd order integration over fibre orientation distributions. In *Proceedings of the international society for magnetic resonance in medicine*, volume 1670. Ismrm, 2010.

[85] Marlene Tahedl, J-Donald Tournier, and Robert E Smith. Structural connectome construction using constrained spherical deconvolution in multi-shell diffusion-weighted magnetic resonance imaging. *Nature Protocols*, pages 1–33, 2025.

[86] Robert E Smith, Jacques-Donald Tournier, Fernando Calamante, and Alan Connelly. Sift2: Enabling dense quantitative assessment of brain white matter connectivity using streamlines tractography. *Neuroimage*, 119:338–351, 2015.

[87] Athena Taymourtash, Ernst Schwartz, Karl-Heinz Nenning, Daniel Sobotka, Roxane Licandro, Sarah Glatter, Mariana Cardoso Diogo, Polina Golland, Ellen Grant, Daniela Prayer, et al. Fetal development of functional thalamocortical and cortico–cortical connectivity. *Cerebral Cortex*, 33(9):5613–5624, 2023.

[88] Alberto Sanfeliu and King-Sun Fu. A distance measure between attributed relational graphs for pattern recognition. *IEEE Transactions on Systems, Man, and Cybernetics*, SMC-13(3):353–362, 1983.

[89] Ali Gholipour, Caitlin K Rollins, Clemente Velasco-Annis, Abdelhakim Ouaalam, Alireza Akhondi-Asl, Onur Afacan, Cynthia M Ortinau, Sean Clancy, Catherine Limperopoulos, Edward Yang, et al. A normative spatiotemporal mri atlas of the fetal brain for automatic segmentation and analysis of early brain growth. *Scientific reports*, 7(1):1–13, 2017.

[90] Richard F Betzel, Alessandra Griffa, Patric Hagmann, and Bratislav Mišić. Distance-dependent consensus thresholds for generating group-representative structural brain networks. *Network neuroscience*, 3(2):475–496, 2019.

[91] Richard F Betzel, John D Medaglia, Lia Papadopoulos, Graham L Baum, Ruben Gur, Raquel Gur, David Roalf, Theodore D Satterthwaite, and Danielle S Bassett. The modular organization of human anatomical brain networks: Accounting for the cost of wiring. *Network neuroscience*, 1(1):42–68, 2017.

[92] Hui Zhang, Paul A Yushkevich, Daniel C Alexander, and James C Gee. Deformable registration of diffusion tensor mr images with explicit orientation optimization. *Medical image analysis*, 10(5):764–785, 2006.

[93] David Raffelt, J-Donald Tournier, Jurgen Fripp, Stuart Crozier, Alan Connelly, and Olivier Salvado. Symmetric diffeomorphic registration of fibre orientation distributions. *Neuroimage*, 56(3):1171–1180, 2011.

[94] Alena Uus, Irina Grigorescu, Maximilian Pietsch, Dafnis Batalle, Daan Christiaens, Emer Hughes, Jana Hutter, Lucilio Cordero Grande, Anthony N Price, Jacques-Donald Tournier, et al. Multi-channel 4d parametrized atlas of macro-and microstructural neonatal brain development. *Frontiers in Neuroscience*, 15:661704, 2021.

[95] Alireza Akhondi-Asl and Simon K Warfield. Simultaneous truth and performance level estimation through fusion of probabilistic segmentations. *IEEE transactions on medical imaging*, 32(10):1840–1852, 2013.

[96] Thijs Dhollander, David Raffelt, and Alan Connelly. Unsupervised 3-tissue response function estimation from single-shell or multi-shell diffusion mr data without a co-registered t1 image. In *ISMRM workshop on breaking the barriers of diffusion MRI*, volume 5. Lisbon, Portugal, 2016.

[97] J-Donald Tournier, Robert Smith, David Raffelt, Rami Tabbara, Thijs Dhollander, Maximilian Pietsch, Daan Christiaens, Ben Jeurissen, Chun-Hung Yeh, and Alan Connelly. Mrtrix3: A fast, flexible and open software framework for medical image processing and visualisation. *Neuroimage*, 202:116137, 2019.

[98] Dmitry Petrov, Alexander Ivanov, Joshua Faskowitz, Boris Gutman, Daniel Moyer, Julio Villalon, Neda Jahanshad, and Paul Thompson. Evaluating 35 methods to generate structural connectomes using pairwise classification. In *International Conference on medical Image Computing and Computer-Assisted Intervention*, pages 515–522. Springer, 2017.

[99] Duncan J Watts and Steven H Strogatz. Collective dynamics of 'small-world'networks. *nature*, 393(6684):440–442, 1998.

[100] Ulrik Brandes. On variants of shortest-path betweenness centrality and their generic computation. *Social networks*, 30(2):136–145, 2008.

[101] Phillip Bonacich. Factoring and weighting approaches to status scores and clique identification. *Journal of mathematical sociology*, 2(1):113–120, 1972.

[102] Martijn P Van Den Heuvel and Olaf Sporns. Rich-club organization of the human connectome. *Journal of Neuroscience*, 31(44):15775–15786, 2011.

[103] Longchuan Li, Xiaoping Hu, Todd M Preuss, Matthew F Glasser, Frederick W Damen, Yuxuan Qiu, and James Rilling. Mapping putative hubs in human, chimpanzee and rhesus macaque connectomes via diffusion tractography. *Neuroimage*, 80:462–474, 2013.

[104] John Darrell Van Horn, Andrei Irimia, Carinna M Torgerson, Micah C Chambers, Ron Kikinis, and Arthur W Toga. Mapping connectivity damage in the case of phineas gage. *PloS one*, 7(5):e37454, 2012.

[105] Emil HJ Nijhuis, Anne-Marie van Cappellen van Walsum, and David G Norris. Topographic hub maps of the human structural neocortical network. *PloS one*, 8(6):e65511, 2013.

[106] Yasser Iturria-Medina, Roberto C Sotero, Erick J Canales-Rodríguez, Yasser Alemán-Gómez, and Lester Melie-García. Studying the human brain anatomical network via diffusion-weighted mri and graph theory. *Neuroimage*, 40(3):1064–1076, 2008.

[107] Gaolang Gong, Yong He, Luis Concha, Catherine Lebel, Donald W Gross, Alan C Evans, and Christian Beaulieu. Mapping anatomical connectivity patterns of human cerebral cortex using in vivo diffusion tensor imaging tractography. *Cerebral cortex*, 19(3):524–536, 2009.

[108] Martijn P Van den Heuvel and Olaf Sporns. Network hubs in the human brain. *Trends in cognitive sciences*, 17(12):683–696, 2013.

[109] Marion I van den Heuvel, Elise Turk, Janessa H Manning, Jasmine Hect, Edgar Hernandez-Andrade, Sonia S Hassan, Roberto Romero, Martijn P van den Heuvel, and Moriah E Thomason. Hubs in the human fetal brain network. *Developmental cognitive neuroscience*, 30:108–115, 2018.

[110] Miao Cao, Yong He, Zhengjia Dai, Xuhong Liao, Tina Jeon, Minhui Ouyang, Lina Chalak, Yanchao Bi, Nancy Rollins, Qi Dong, et al. Early development of functional network segregation revealed by connectomic analysis of the preterm human brain. *Cerebral cortex*, 27(3):1949–1963, 2017.

[111] Miao Cao, Hao Huang, Yun Peng, Qi Dong, and Yong He. Toward developmental connectomics of the human brain. *Frontiers in neuroanatomy*, 10:25, 2016.

[112] Gareth Ball, Paul Aljabar, Sally Zebari, Nora Tusor, Tomoki Arichi, Nazakat Merchant, Emma C Robinson, Enitan Ogundipe, Daniel Rueckert, A David Edwards, et al. Rich-club organization of the newborn human brain. *Proceedings of the National Academy of Sciences*, 111(20):7456–7461, 2014.

[113] Hao Huang, Ni Shu, Virendra Mishra, Tina Jeon, Lina Chalak, Zhiyue J Wang, Nancy Rollins, Gaolang Gong, Hua Cheng, Yun Peng, et al. Development of human brain structural networks through infancy and childhood. *Cerebral Cortex*, 25(5):1389–1404, 2015.

[114] Wei Gao, Hongtu Zhu, Kelly S Giovanello, J Keith Smith, Dinggang Shen, John H Gilmore, and Weili Lin. Evidence on the emergence of the brain's default network from 2-week-old to 2-year-old healthy pediatric subjects. *Proceedings of the National Academy of Sciences*, 106(16):6790–6795, 2009.

[115] Wei Gao, John H Gilmore, Kelly S Giovanello, Jeffery Keith Smith, Dinggang Shen, Hongtu Zhu, and Weili Lin. Temporal and spatial evolution of brain network topology during the first two years of life. *PloS one*, 6(9):e25278, 2011.

[116] Peter Fransson, Ulrika Åden, Mats Blennow, and Hugo Lagercrantz. The functional architecture of the infant brain as revealed by resting-state fmri. *Cerebral cortex*, 21(1):145–154, 2011.

[117] Moriah E Thomason, Jesse A Brown, Maya T Dassanayake, Rupal Shastri, Hilary A Marusak, Edgar Hernandez-Andrade, Lami Yeo, Swati Mody, Susan Berman, Sonia S Hassan, et al. Intrinsic functional brain architecture derived from graph theoretical analysis in the human fetus. *PLoS one*, 9(5):e94423, 2014.

[118] Camilo Calixto, Matheus Dorigatti Soldatelli, Camilo Jaimes, Lana Pierotich, Simon K Warfield, Ali Gholipour, and Davood Karimi. A detailed spatiotemporal atlas of the white matter tracts for the fetal brain. *Proceedings of the National Academy of Sciences*, 122(1):e2410341121, 2025.

[119] Ruike Chen, Cong Sun, Tingting Liu, Yuhao Liao, Junyan Wang, Yi Sun, Yi Zhang, Guangbin Wang, and Dan Wu. Deciphering the developmental order and microstructural patterns of early white matter pathways in a diffusion mri based fetal brain atlas. *Neuroimage*, 264:119700, 2022.

[120] Joana Sa de Almeida, Djalel-Eddine Meskaldji, Serafeim Loukas, Lara Lordier, Laura Gui, Francois Lazeyras, and Petra S Hüppi. Preterm birth leads to impaired rich-club organization and fronto-paralimbic/limbic structural connectivity in newborns. *NeuroImage*, 225:117440, 2021.

[121] Nagulan Ratnarajah, Anne Rifkin-Graboi, Marielle V Fortier, Yap Seng Chong, Kenneth Kwek, Seang-Mei Saw, Keith M Godfrey, Peter D Gluckman, Michael J Meaney, and Anqi Qiu. Structural connectivity asymmetry in the neonatal brain. *Neuroimage*, 75:187–194, 2013.

[122] Dafnis Batalle, Emer J Hughes, Hui Zhang, J-Donald Tournier, Nora Tusor, Paul Aljabar, Luqman Wali, Daniel C Alexander, Joseph V Hajnal, Chiara Nosarti, et al. Early development of structural networks and the impact of prematurity on brain connectivity. *Neuroimage*, 149:379–392, 2017.

[123] Mark D Humphries, Kevin Gurney, and Tony J Prescott. The brainstem reticular formation is a small-world, not scale-free, network. *Proceedings of the Royal Society B: Biological Sciences*, 273(1585):503–511, 2006.

[124] Qawi K Telesford, Karen E Joyce, Satoru Hayasaka, Jonathan H Burdette, and Paul J Laurienti. The ubiquity of small-world networks. *Brain Connectivity*, 2011.

[125] Zachary P Neal. How small is it? comparing indices of small worldliness. *Network Science*, 5(1):30–44, 2017.

[126] Feng Shi, Pew-Thian Yap, Wei Gao, Weili Lin, John H Gilmore, and Dinggang Shen. Altered structural connectivity in neonates at genetic risk for schizophrenia: a combined study using morphological and white matter networks. *Neuroimage*, 62(3):1622–1633, 2012.

[127] Bahram Marami, Seyed Sadegh Mohseni Salehi, Onur Afacan, Benoit Scherrer, Caitlin K Rollins, Edward Yang, Judy A Estroff, Simon K Warfield, and Ali Gholipour. Temporal slice registration and robust diffusion-tensor reconstruction for improved fetal brain structural connectivity analysis. *NeuroImage*, 156:475–488, 2017.